



## Article

# Estimation of Arctic Sea Ice Thickness from Chinese HY-2B Radar Altimetry Data

Maofei Jiang <sup>1,\*</sup> , Wenqing Zhong <sup>1,2</sup>, Ke Xu <sup>1</sup> and Yongjun Jia <sup>3,4</sup>

<sup>1</sup> The CAS Key Laboratory of Microwave Remote Sensing, National Space Science Center, Chinese Academy of Sciences (CAS), Beijing 100190, China

<sup>2</sup> University of Chinese Academy of Sciences, Beijing 100049, China

<sup>3</sup> Key Laboratory of Space Ocean Remote Sensing and Application, Ministry of Natural Resources, Beijing 100081, China

<sup>4</sup> National Satellite Ocean Application Service, Beijing 100081, China

\* Correspondence: jiangmaofei@mirslab.cn

**Abstract:** Sea ice thickness (SIT) is an important parameter in the study of climate change. During the past 20 years, satellite altimetry has been widely used to observe sea ice thickness. The Chinese Haiyang-2B (HY-2B) radar altimeter, launched in October 2018, can provide data up to 80.6° latitude and can be used as a supplementary means to observe polar sea ice. Reliable HY-2B SIT products will contribute to the sea ice community. In this study, we aimed to assess the Arctic sea ice thickness retrieval ability of the HY-2B radar altimetry data. We processed the HY-2B radar altimetry data from January 2019 to April 2022 and used the processed data to retrieve the Arctic SIT. The Alfred Wegener Institute (AWI) CryoSat-2 (CS-2) SIT products were used to calibrate the HY-2B SIT estimates with a linear regression method. The Goddard Space Flight Center (GSFC) CS-2, Jet Propulsion Laboratory (JPL), and GSFC ICESat-2 (IS-2) SIT products were used to validate the HY-2B calibrated SIT estimates. The HY-2B calibrated SIT estimates have good, consistent spatial distributions with the CS-2 and IS-2 SIT products. The comparison with the IS-2 and IS-2 SIT products shows the root-mean-square error (RMSE) and bias for the HY-2B SIT estimates are significantly reduced after calibration. The HY-2B SIT estimates were also validated using the ice thickness data from Operation IceBridge (OIB) and the ice draft data from the Beaufort Gyre Exploration Project (BGEF). Finally, the monthly variations of the HY-2B SIT estimates were analyzed. Results show that the HY-2B calibrated SIT estimates are reliable, especially when the SIT values are lower than 3 m. The HY-2B altimetry data is a possible source for sea ice thickness data at lower latitudes and will help us better understand the sea ice response to climate change.

**Keywords:** HY-2B; radar altimeter; Arctic; sea ice thickness



**Citation:** Jiang, M.; Zhong, W.; Xu, K.; Jia, Y. Estimation of Arctic Sea Ice Thickness from Chinese HY-2B Radar Altimetry Data. *Remote Sens.* **2023**, *15*, 1180. <https://doi.org/10.3390/rs15051180>

Academic Editor: Gareth Rees

Received: 2 January 2023

Revised: 14 February 2023

Accepted: 19 February 2023

Published: 21 February 2023



**Copyright:** © 2023 by the authors. Licensee MDPI, Basel, Switzerland. This article is an open access article distributed under the terms and conditions of the Creative Commons Attribution (CC BY) license (<https://creativecommons.org/licenses/by/4.0/>).

## 1. Introduction

In recent years, global climate change has become a research topic attracting worldwide attention. Sea ice is one of the most important environmental factors in the climate system [1]. Sea ice changes affect regional and global climate, and climate changes further change the characteristics of sea ice. Sea ice thickness is particularly significant and sensitive to the coupling effect of the atmosphere, sea ice, and ocean and directly determines the process and rate of energy and material exchange between sea and air [2]. It dominates the thermodynamics and dynamics of sea ice and then feeds back to the global climate system, environmental system, and ecosystem, causing a series of changes in climate and environmental parameters related to human survival [3].

Over the past 20 years, satellite altimetry has become the most widely used method to measure sea ice thickness. Compared with other observation methods, the advantage of satellite altimetry is that it can obtain hemispherical SIT information. Laxon et al. [4] first used ERS-1/2 and Envisat radar altimeter data to retrieve the sea ice thickness, then

confirmed the feasibility of retrieving large-scale sea ice thickness by satellite altimeter data with submarine sonar data. Since then, satellite radar altimeters, such as Envisat [5,6], Cryosat-2 [7,8] and Sentinel-3A/B [9], and laser altimeters, such as ICESat-1 [10–12] and ICESat-2 [13,14] have been used to estimate the sea ice thickness.

The HY-2B satellite is China's second marine dynamic environment detection satellite [15]. It was launched on 25 October 2018, and is in a sun-synchronous orbit with a 973 km orbital height. HY-2B, together with HY-2C (launched on 21 September 2020) and HY-2D (launched on 19 May 2021), forms China's first marine dynamic environment satellite constellation and greatly improves the global observation coverage and timeliness of marine dynamic environmental elements. HY-2B is a polar orbit satellite (inclination: 99.3°), while both HY-2C and HY-2D are inclined orbit satellites (inclination: 66°).

The dual-frequency radar altimeter (Ku band: 13.58 GHz and C band: 5.25 GHz) is one of HY-2B's main payloads. The HY2B radar altimeter is the first radar altimeter to use the rubidium clock as a frequency reference source. Due to the high stability of the rubidium clock, the range drifts of the HY-2B radar altimeter will be no more than 0.1 mm/year [16]. Similar to the Envisat and Jason-1/2/3 radar altimeters, the HY-2B radar altimeter adopts the pulse-limited operation mode to measure the sea surface height, significant wave height, and sea surface wind speed. Due to its high quality over the ocean, the HY-2B radar altimetry data has been successfully integrated into the Data Unification and Altimeter Combination System (DUACS) [17]. However, the HY-2B radar altimetry data are rarely used in polar sea ice research. The HY-2B radar altimeter can provide measurements up to 80.6° latitude and can be used as a supplementary means to observe polar sea ice. Reliable HY-2B SIT products are important for providing sea ice thickness data at lower latitudes and will help us better understand the sea ice response to climate change.

In this study, we aimed to assess the Arctic sea ice thickness retrieval ability of the HY-2B radar altimetry data. We processed the HY-2B radar altimetry data from January 2019 to April 2022 and used the processed data to estimate the Arctic sea ice thickness. The AWI CS-2 SIT products were used to calibrate the HY-2B SIT estimates. Additionally, we validated the HY-2B SIT estimates by comparison with the GSFC CS-2 SIT products, the JPL and GSFC IS-2 SIT products, OIB airborne data, and BGEP sea ice draft data.

## 2. Materials and Methods

### 2.1. HY-2B Radar Altimetry Data

The radar altimeter onboard HY-2B operates in the Ku and C bands. It is a conventional pulse-limited altimeter. The pulse-limited footprint diameters of the Ku and C bands are 1.9 km and 10 km, respectively. The C-band data are mainly used for ionospheric corrections. In this study, we only used Ku-band data. The main characteristics of the HY-2B radar altimeter are listed in Table 1. The orbit inclination of the HY-2B satellite is 99.3°, and the repeat cycle is 14 days.

**Table 1.** HY-2B radar altimeter parameter [16].

Parameter	Value
Emission signal center frequency	13.58 GHz (Ku), 5.25 GHz (C)
Orbit altitude	973 km
Orbit inclination angle	99.3°
Orbit period	14 days
Number of range bin	128
Transmission pulse width	102.4 μs
Ku pulse repetition rate	2 kHz
Antenna aperture	1.3 m
Bandwidth	320 MHz
Ground footprint diameter	1.9 km (Ku), 10 km (C)

The HY-2B radar altimeter uses both Sub-optimal Maximum likelihood Estimate (SMLE) and off-center of gravity (OCOG) tracking modes. Figure 1 shows the distribution area of the two tracking modes over the Arctic Ocean in January 2021. For areas with slower changes in terrain height, such as the ocean and large areas of flat sea ice, the SMLE tracking mode is used. For areas with more dramatic changes in topographic height, such as land and sea ice areas, the OCOG tracking mode is used. The currently released HY-2B L2 altimetry products only contain data from the SMLE tracking packages, while the L1 products contain data from both tracking modes. In this study, we processed the HY-2B L1 altimetry data from January 2019 to April 2022 to estimate the Arctic SIT. The HY-2B altimetry data could be obtained from the National Satellite Ocean Application Service (NSOAS).

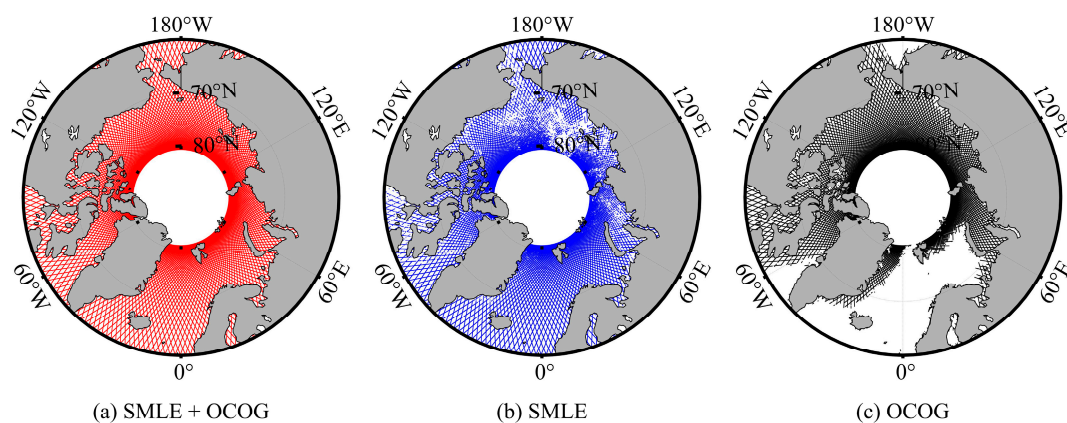


**Figure 1.** Distribution of HY-2B altimeter data for two tracking modes over the Arctic Ocean in January 2021.

## 2.2. Cryosat-2 SIT Data

In April 2010, the European Space Agency successfully launched the CryoSat-2 (CS-2) satellite, which is mainly used for the measurement of sea ice thickness and ice sheet elevation. The satellite flies in a non-sun-synchronous orbit with an altitude of about 717 km, a repeat cycle of 369 days, an orbital inclination of  $92^\circ$ , and data coverage of  $88^\circ$  north and south latitude.

CS-2 is equipped with the SAR Interferometric Radar Altimeter (SIRAL). The design of SIRAL is derived from the traditional pulse-limited radar altimeter and combined with synthetic aperture and interferometric signal processing technology. It can achieve accurate measurement of the ice sheet edge and systematic detection of changes in sea ice freeboard height. SIRAL operates in three main observation modes, of which the low-resolution mode (LRM) is mainly used to measure the inland ice sheet with a small slope; the SAR mode is mainly used to measure sea ice; the SARIn mode is mainly used to measure the edge of the ice sheet with a large slope. In SAR mode, SIRAL uses the along-track beam formation to generate a much smaller footprint strip (about 300 m along track and 1.6 km cross-track) than the circular footprint ( $\sim 2$  km diameter) of the conventional pulse-limited altimeters such as Envisat, Jason-1/2/3, and HY-2B altimeters.

Several institutions, such as the Centre for Polar Observation and Modelling (CPOM) [18], the NASA Goddard Space Flight Center (GSFC) [19], the Alfred Wegener Institut (AWI) [20] have used the CS-2 altimetry data to retrieve the Arctic SIT and publicly released their products. Different institutions use different methods to process the CS-2 data. CPOM uses a Gaussian-exponential retracker and a threshold retracker to process the lead and sea ice waveforms, respectively. AWI applies a threshold retracker to process all waveforms. GSFC uses a waveform-fitting model to process both lead and sea ice waveforms.

Similar to the AWI CS-2 SIT products, we also used a threshold method to retrack the HY-2B radar altimeter waveforms. Therefore, we used the AWI CS-2 SIT products to calibrate and validate the HY-2B SIT estimates. In addition, we also used the GSFC CS-2 SIT products to validate our results.

### 2.3. ICESat-2 SIT Data

In September 2018, NASA launched the ICESat-2 (IS-2) satellite. The observation range of IS-2 is between 88° south and north latitude. IS-2's repeat cycle is 91 days, and the mean orbit altitude is ~500 km. The Advanced Topographic Laser Altimeter System (ATLAS) is IS-2's main payload. ATLAS emits pulses with a laser wavelength of 532 nm at a frequency of 10 kHz. The emitted laser beams are divided into six beams, three pairs of strong and weak beams are arranged in parallel along the orbit, with the spacing between groups of about 3.3 km. The vertical spacing of strong and weak beams in each pair of orbits is 90 m; the vertical spacing of strong and weak beams along the orbit is 2.5 km; the spot diameter is about 17 m; and the spatial resolution of the satellite along the orbit is 70 cm [21].

NASA GFSC publicly released the IS-2 L4 Monthly Gridded SIT (IS2SITMOGR4) products. IS2SITMOGR4 uses ATLAS ATL10 products to estimate the winter Arctic SIT [13]. The Jet Propulsion Laboratory (JPL) also retrieved the Arctic SIT using the ATLAS ATL10 snow-freeboard products [22]. In this study, we also used the GSFC and JPL IS-2 SIT products to validate the HY-2B SIT estimates. There are some differences between the GSFC and JPL IS-2 products. GSFC uses the snow loading estimates from the NASA Eulerian Snow on Sea Ice Model (NESOSIM) to estimate the SIT, while JPL uses the snow depth derived from IS-2 and CS-2 [23].

### 2.4. OIB SIT Data

Operation IceBridge (OIB) has been an important polar airborne observation project for NASA in recent years. The IceBridge project aims to fill the data gap between the laser altimetry satellites ICESat and ICESat-2 to ensure continuous observation in the polar regions [24]. From January 2019 to now, only the OIB data from April 2019 can be used to validate the HY-2B SIT estimates, and their tracks are shown in Figure 2a. In this study, the IceBridge L4-level (IDCSI4) data were used to validate the HY-2B SIT estimates. The OIB SIT data were gridded to a 25 km EASE2 grid.

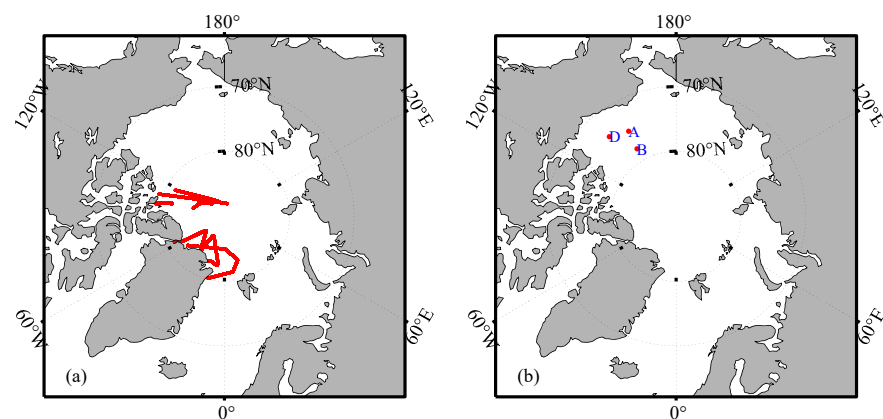


**Figure 2.** The (a) OIB tracks in April 2019 and (b) locations of the three ULNs of BGEP.

### 2.5. BGEP Ice Draft Data

The ice draft data derived from three moored upward-looking sonars (ULN) of the Beaufort Gyre Exploration Project (BGEP) [25] were also used to validate the HY-2B SIT estimates. We used the daily average draft data from moorings A, B, and D. The locations of moorings A, B, and D are shown in Figure 2b.

### 2.6. Auxiliary Data

In this study, we used daily sea ice concentration products and sea ice type products from the EUMETSAT Marine and Sea Ice Satellite Application Facility (OSI-SAF). The AWI snow depth data fusing the W99 climatology snow depths and the AMSR-2 snow depths [26] were used to estimate the HY-2B SIT.

2.7. Sea Ice Thickness Retrieval Method

Figure 3 shows the sea ice thickness retrieval flow chart based on the HY-2B radar altimetry data. The surface height measured by the HY-2B radar altimeter is expressed as follows [27]:

$$h = H - (R + \Delta R_{corr}) \tag{1}$$

$$\Delta R_{corr} = \Delta R_{dry} + \Delta R_{wet} + \Delta R_{iono} + \Delta R_{ocean} + \Delta R_{solid} + \Delta R_{pole} + \Delta R_{DAC} \tag{2}$$

where  $H$  is the altitude of the satellite,  $R$  is the distance from the satellite to the earth's surface, and  $\Delta R_{corr}$  contains the range and geophysical error corrections.  $\Delta R_{dry}$  is the dry wet troposphere correction,  $\Delta R_{wet}$  is the wet troposphere correction,  $\Delta R_{iono}$  is the ionosphere correction,  $\Delta R_{ocean}$  is the geocentric ocean tide,  $\Delta R_{solid}$  is the solid earth tide,  $\Delta R_{pole}$  is the pole tide, and  $\Delta R_{DAC}$  is the dynamic atmosphere correction.

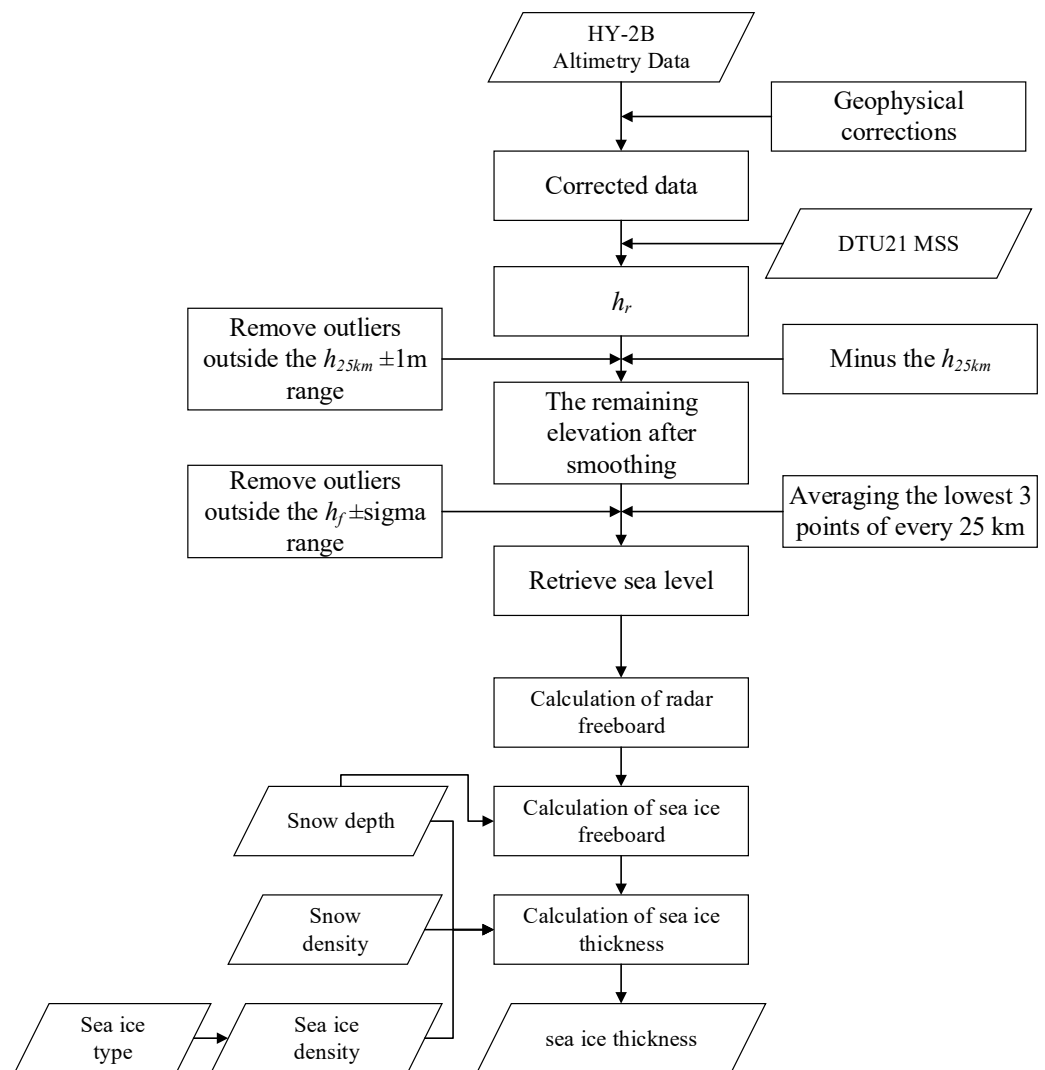


Figure 3. Sea ice thickness retrieval flow chart based on the HY-2B radar altimetry data.

The Threshold First Maximum Retracker Algorithm (TFMRA) [28] was applied to process the HY-2B altimeter waveforms. We adopted a 50% threshold. The dry troposphere correction was calculated as follows [29]:

$$\Delta R_{dry} = - \frac{0.0022768 P_s}{1 - 0.00266 \cos 2\varphi - 0.28 \cdot 10^{-6} z_s} \tag{3}$$

where  $P_s$  is the surface pressure at height  $z_s$  above the geoid, and  $\varphi$  is the geodetic latitude. In this study,  $P_s$  is derived from the surface pressure data from the National Centers for Environmental Prediction (NCEP) FNL (Final) operational global analysis data using linear interpolation.

The wet troposphere correction was computed as follows [29]:

$$\Delta R_{wet} = -(a_0 + a_1 TCWV + a_2 TCWV^2 + a_3 TCWV^3) TCWV \cdot 10^{-2} \quad (4)$$

where  $TCWV$  is the total column water vapor,  $a_0 = 6.8544$ ,  $a_1 = -0.4377$ ,  $a_2 = 0.0714$ ,  $a_3 = -0.0038$ . We obtained  $TCWV$  from the NCEP FNL operational global analysis data using linear interpolation.

The ionosphere correction was computed as follows [30]:

$$\Delta R_{iono} = -\frac{k \cdot c_{te}}{f^2} \quad (5)$$

where  $k = 0.40250 \times 10^{-6}$ ,  $c_{te}$  is the total electron content (TEC),  $f$  is the electromagnetic radiation frequency. In this study, the JPL-GIM TEC data [31] were used to calculate the total electron content with linear interpolation.

The geocentric ocean tide correction was computed using the FES2014 ocean tide model [32]. The dynamic atmosphere correction was calculated using the two-dimensional Gravity Waves model (MOG2D) data with linear interpolation [33]. The solid earth tide was calculated using the method developed by Cartwright and Edden [34]. The pole tide was computed using the earth orientation data from the International Earth Rotation Service (IERS) with the method described by Wahr [35].

The mean sea surface (MSS) was applied to remove the geoid undulations:

$$h_r = h - h_{mss} \quad (6)$$

where  $h_r$  is the relative surface height and  $h_{mss}$  is the mean sea surface. We used the DTU21 MSS model [36] to calculate the mean sea surface.

Kwok et al. [37] found that the residuals in sea surface height are much greater than the expected magnitude of sea ice freeboard and used a 25 km running mean of  $h_r$  to remove the residuals. We followed Kwok's method to obtain the modified relative surface height. The relative surface height  $h_r$  was filtered through the sliding average of 25 km and the modified relative surface height is obtained by [37]:

$$h'_r = h_r - h_{25km} \quad (7)$$

where  $h_{25km}$  is the filtered  $h_r$ . Figure 4 shows a sample of the HY-2B elevation profiles of  $h_r$  and  $h'_r$  over the Arctic ocean.

The freeboard is usually derived from the elevation difference between the sea ice surface and the local sea surface. The local sea surface height can be regarded as the leading elevation in sea ice-covered areas. Lindsay and Rothrock [38] found that leads cover 2–3% of the sea ice cover of the Arctic Ocean. Kwok et al. [37] developed a convenient method to calculate the lead elevation. Leads were considered to be at sea level, and the sea surface height at any given point was derived by averaging the lowest 2% of the ICESat elevations within 25 km of that point. Zwally et al. [39] detected leads in at least 2% of a 50 km section of an ICESat elevation profile and calculated the sea surface height by averaging the lowest 2% of the relative elevations. Skorup et al. [40] calculated the sea surface height by averaging the three lowest elevations in a 20 km section of an ICESat profile. Zhang et al. [41] calculated the sea surface height by averaging the three lowest elevations in a 25 km section of an Envisat profile. We followed Zhang's method to compute the sea surface height by averaging the three lowest  $h'_r$  per 25 km. The radar freeboard is computed as follows:

$$h_f = h'_r - h_{ssh} \quad (8)$$

where  $h_f$  is the radar freeboard,  $h'_r$  is the modified relative surface height, and  $h_{ssh}$  is the sea surface height. Figure 5 shows a sample of the HY-2B elevation profiles of  $h'_r$ ,  $h_{ssh}$  and  $h_f$  over the Arctic ocean.

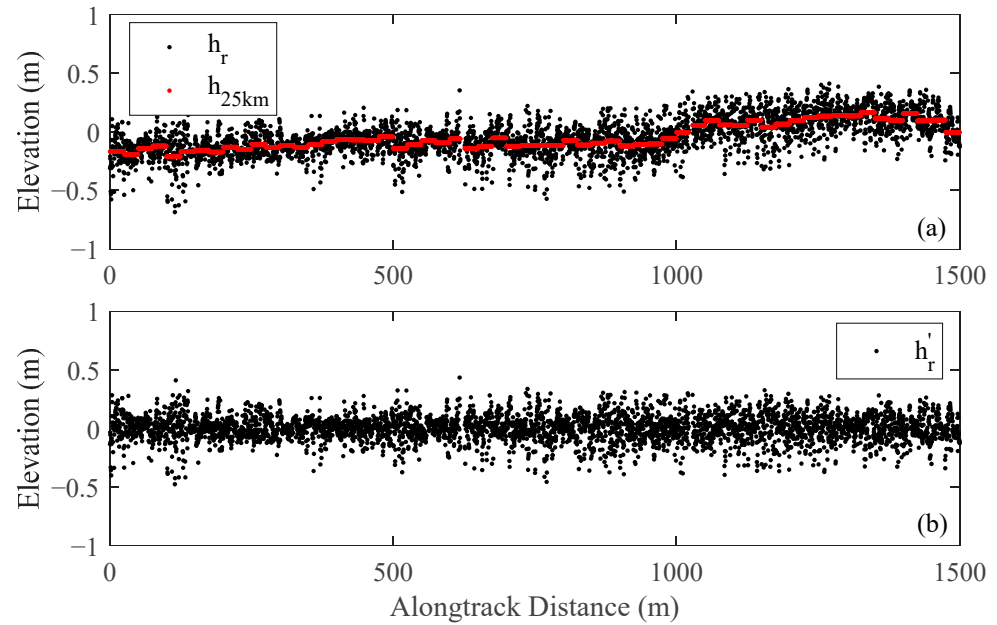


**Figure 4.** A sample of the HY-2B elevation profiles of (a)  $h_r$ ,  $h_{25km}$  and (b)  $h'_r$  over the Arctic Ocean.

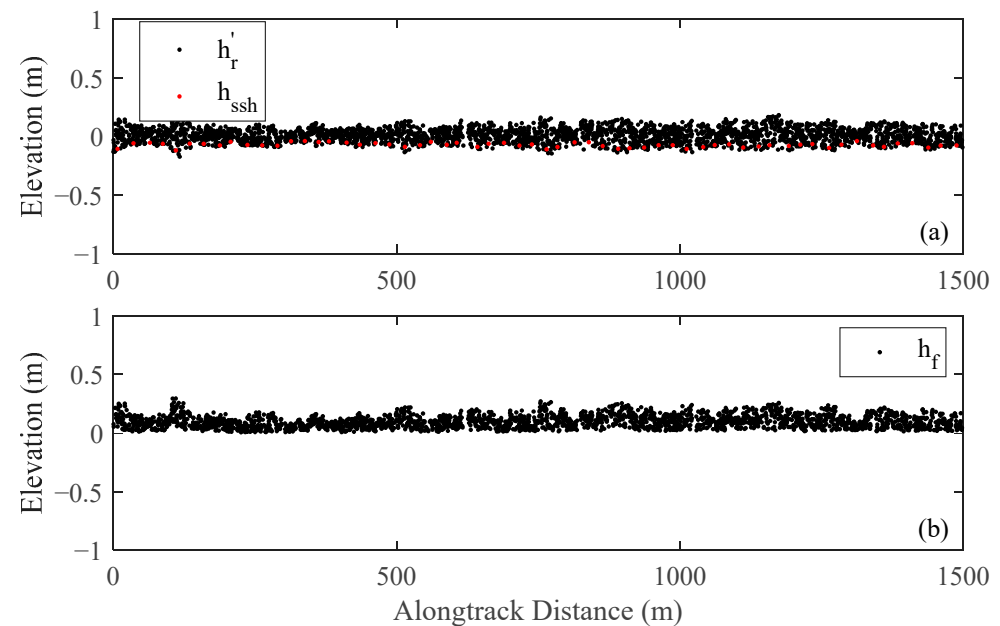


**Figure 5.** A sample of the HY-2B elevation profiles of (a)  $h'_r$ ,  $h_{ssh}$  and (b)  $h_f$  over the Arctic Ocean.

Radar signals travel slower in snow than in a vacuum. The radar freeboard should be corrected using the snow depth  $h_s$  to derive the sea ice freeboard  $h_{fi}$  [8,42]:

$$h_{fi} = h_f + h_s \left( \frac{c}{c_s} - 1 \right) \quad (9)$$

$$c_s = c(1 + 5.1 \times 10^{-4} \rho_s)^{-1.5} \quad (10)$$

where  $c$  is the speed of light,  $c_s$  is the speed of light through snow, and  $\rho_s$  is the snow density.

Sea ice thickness was finally estimated from the sea ice freeboard [7]:

$$h_i = \frac{h_{fi}\rho_w + h_s\rho_s}{\rho_w - \rho_i} \quad (11)$$

where  $h_i$  is the sea ice thickness,  $h_{fi}$  is the corrected sea ice freeboard,  $h_s$  is the snow depth,  $\rho_w$  is seawater density ( $1024 \text{ kg m}^{-3}$ ),  $\rho_s$  is the snow density, and  $\rho_i$  is sea ice density. For the first-year ice (FYI),  $\rho_i$  is  $916.7 \text{ kg m}^{-3}$  while for the multi-year ice (MYI),  $882.0 \text{ kg m}^{-3}$  is used. The snow density  $\rho_s$  is computed as follows [42]:

$$\rho_s = 6.5 \times t + 274.51 \quad (12)$$

where  $t$  is the number of months since October.

### 3. Results

#### 3.1. Comparison against the IS-2 SIT Data

We first estimated the monthly Arctic SIT using the reprocessed HY-2B altimetry data from October 2021 to April 2022 and then used the AWI CS-2 SIT to calibrate our results. The SIT estimates were projected to a 25 km EASE2 grid. Figure 6a shows the scatterplots of the HY-2B SIT estimates against the results from the AWI CS-2 products. Figure 6b shows the histograms of the SIT biases between HY-2B and AWI CS-2 SIT estimates. The SIT biases have near-normal distributions. Compared to the AWI CS-2 products, the HY-2B SIT estimates have an RMSE of 1.19 m with a positive bias of 1.08 m. The mean relative error (MRE) is 1.47. As shown by Zhang et al. [41], the Envisat sea ice freeboard estimates have a positive bias of 0.12 m against the AWI CS-2 products. The method used to derive the HY-2B sea ice freeboard in this study is the same as the method used by Zhang et al. [41]. Therefore, the method used in this study may overestimate the sea ice freeboard values and thus overestimate the SIT values. There may be several reasons for the differences between the HY-2B SIT estimates and the AWI CS-2 SIT estimates. Firstly, the HY-2B altimeter operates in LRM mode while the CS-2 altimeter operates mainly in SAR mode over Arctic sea ice. Secondly, our method of retrieving the freeboard is different from the AWI CS-2 SIT products. For the AWI CS-2 SIT products, leads are detected from waveform parameters such as pulse peakiness and stack standard deviation, and the sea surface height is calculated from the lead waveforms. However, we computed the sea surface height by averaging the three lowest elevations in a 25 km section of an HY-2B profile. Moreover, the MSS model we used is also different from the one for the AWI CS-2 SIT products.

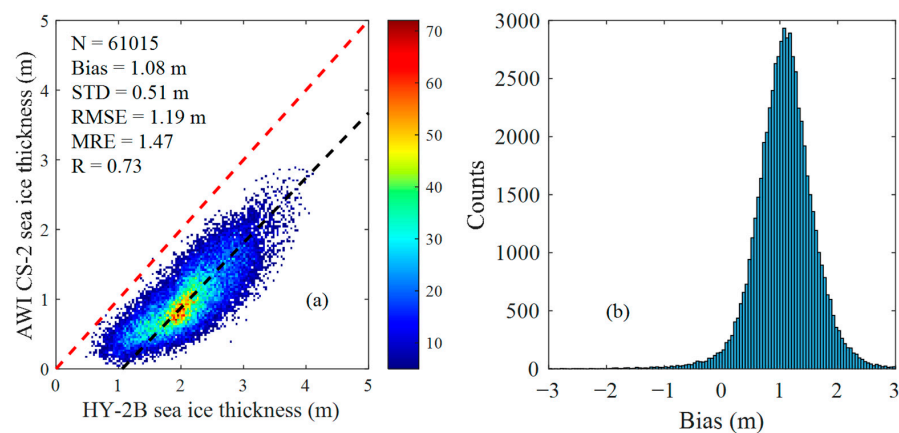


**Figure 6.** Comparison of the SIT estimates between the HY-2B and AWI CS-2 SIT products: (a) scatterplot and (b) histogram of the differences between the two products.

For the AWI CS-2 SIT products, the altimeter waveforms are processed using the threshold method. In this study, we also used a threshold method to process the HY-2B

altimeter waveforms. Moreover, the seawater density, sea ice density and snow density, used to estimate the SIT in this study are the same as those for the AWI CS-2 SIT products. Therefore, we used the AWI CS-2 SIT products to calibrate the HY-2B SIT estimates. We use a linear regression method to calibrate the HY-2B SIT estimates:

$$SIT_{HY2B}^{corrected} = \alpha \times SIT_{HY2B}^{raw} + \beta \quad (13)$$

where  $SIT_{HY2B}^{raw}$  is the derived HY-2B SIT value,  $SIT_{HY2B}^{corrected}$  is the corrected HY-2B SIT value,  $\alpha$  and  $\beta$  are the regression coefficients. The HY-2B and AWI CS-2 SIT estimates from October 2021 to April 2022 were used to calculate the regression coefficients. The correction model may depend on the ice thickness and the physical characteristics of snow and sea ice. Therefore, we established different correction models based on the data from different months. Table 2 shows the regression coefficients for different months.

**Table 2.** The regression coefficients  $\alpha$  and  $\beta$  for different months.

	October	November	December	January	February	March	April
$\alpha$	0.83	0.88	0.87	0.90	0.93	0.93	0.94
$\beta$	−0.82	−0.91	−0.88	−0.92	−0.96	−0.96	−1.00

Monthly SIT for HY-2B and CS-2 are shown for the 2020–2021 winter season in Figure 7. The differences between the HY-2B SIT estimates and the AWI and GSFC CS-2 SIT estimates are also shown in Figure 7. Along-track SIT measurements for the month were projected to a 25 km EASE2 grid after 3-sigma filtering. The HY-2B SIT estimates are higher than the CS-2 SIT estimates for all months. Figure 8 shows the results of the HY-2B calibrated SIT estimates. After calibration, the HY-2B SIT estimates are more consistent with those of the AWI and GSFC CS-2 SIT products. Thicker sea ice appears in the Beaufort Sea and north of the Canadian Arctic Archipelago, while thinner sea ice appears in the East Siberian and Barents Seas. In addition, the HY-2B and CS-2 SIT products showed similar seasonal changes in which the Arctic SIT gradually thickened. The HY-2B calibrated SIT estimates are higher than those of AWI and GSFC CS-2 SIT products in the Beaufort Sea and north of the Canadian Arctic Archipelago, where the SIT values are thicker than in other areas.

Figure 9 shows the comparison of the HY-2B SIT estimates and the two CS-2 SIT products for the period January 2019 to April 2021. Compared to the AWI CS-2 SIT products, the HY-2B SIT estimates have an RMSE of 1.33 m, with a positive bias of 1.19 m, and an MRE of 1.53. After calibration, the RSME, bias, and MRE for the HY-2B SIT estimates are reduced to 0.53 m, 0.08 m, and 0.41, respectively. The STD of the differences between the HY-2B calibrated SIT estimates and the AWI CS-2 SIT products is 0.53 m, which is slightly lower than the value without calibration (0.58 m). The correlation coefficient between the HY-2B calibrated SIT estimates and the AWI CS-2 SIT products is 0.66, which is the same as the value without calibration. Compared to the GSFC CS-2 SIT products, the HY-2B calibrated SIT estimates have an RMSE of 0.61 m with a negative bias of 0.28 m, and the correlation coefficient and MRE are 0.53 and 0.30, respectively.

To analyze the performance of the HY-2B SIT estimates in different SIT ranges, we computed the biases between the HY-2B and the two CS-2 products into six SIT ranges. Table 3 shows the statistics of the biases between the HY-2B estimates and the two CS-2 products in different SIT ranges. Compared to the AWI CS-2 products, the biases are mainly distributed in thin-ice-covered areas (SIT smaller than 1 m). The HY-2B estimates have a 1.18 m bias against the AWI CS-2 products and a 0.92 m bias against the GSFC CS-2 products when SIT is smaller than 1 m. After calibration, the biases for the HY-2B estimates are reduced to 0.08 m for the AWI CS-2 products and −0.19 m for the GSFC CS-2 products, respectively. The bias between the HY-2B SIT estimates and the AWI CS-2 SIT products is smallest in areas of SIT larger than 3 m and smaller than 4 m. After the HY-2B SIT estimates are calibrated, the biases increase with SIT in areas with SIT greater than 1 m. The STD and

RMSE for the HY-2B calibrated SIT estimates increase with SIT when compared against both AWI and GSFC CS-2 products. At high SIT values (when SIT is larger than 3 m), the HY-2B calibrated SIT estimates significantly underestimate the SIT.

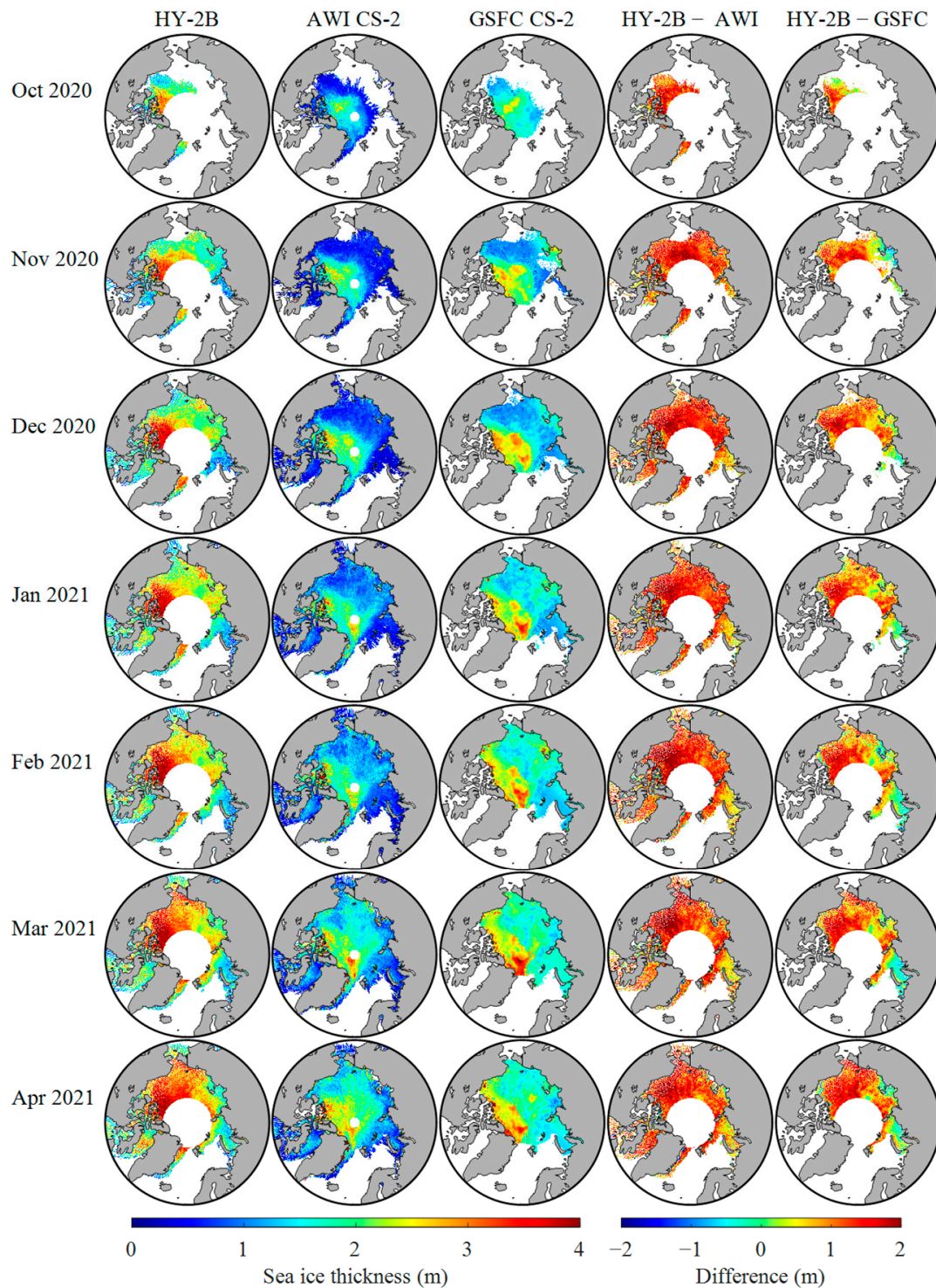


**Figure 7.** Comparison of the HY-2B SIT, AWI CS-2 SIT, GSFC CS-2 SIT, HY-2B minus AWI CS-2 SIT, and GSFC CS-2 SIT from October 2020 to April 2021.

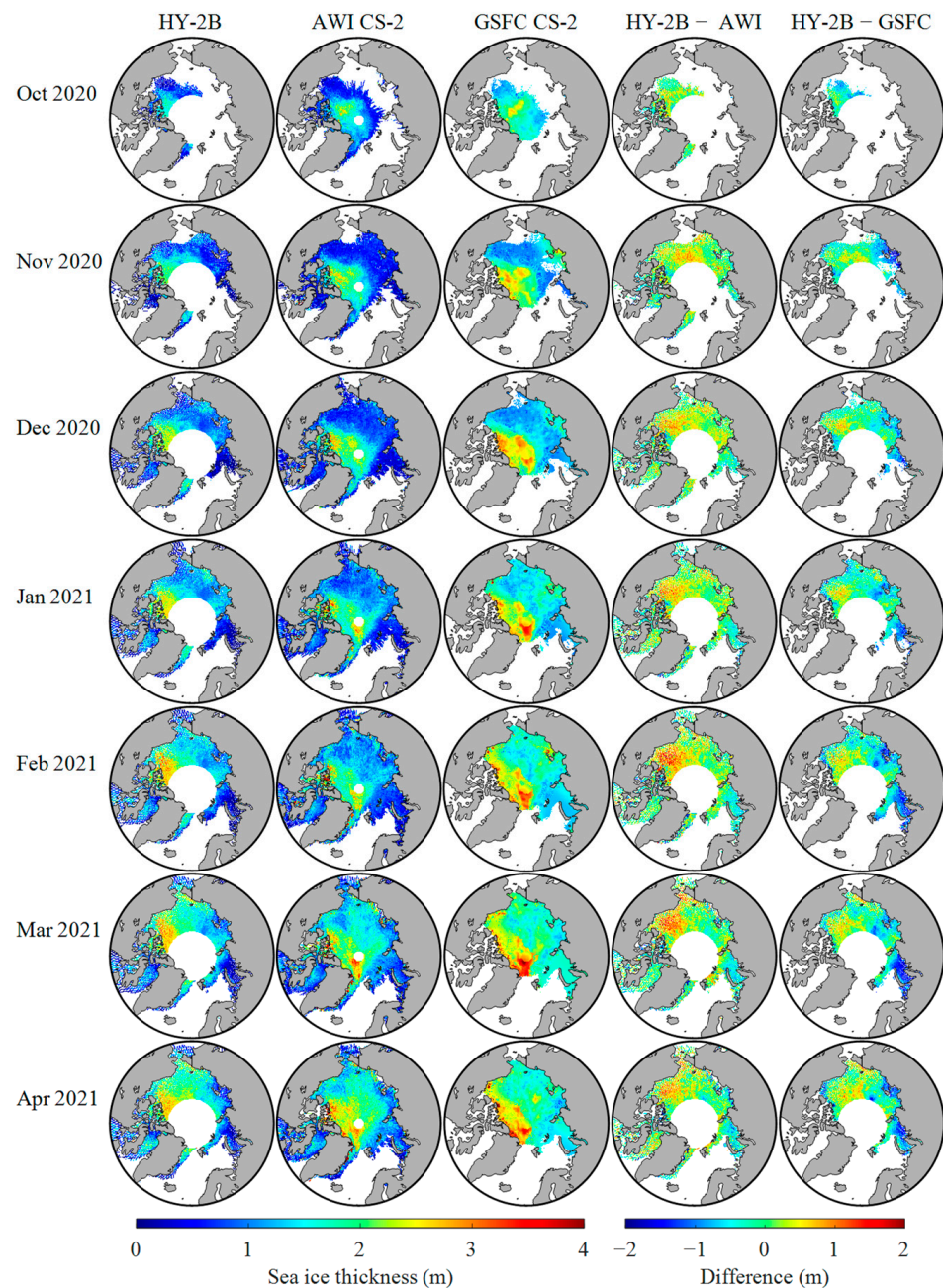


**Figure 8.** Comparison of the HY-2B calibrated SIT, AWI CS-2 SIT, GSFC CS-2 SIT, HY-2B calibrated SIT minus AWI CS-2 SIT, and GSFC CS-2 SIT from October 2020 to April 2021.

To assess the bias between the HY-2B and the two CS-2 SIT estimates on various sea ice types, we list the biases in FYI, MYI, and total sea ice between the monthly average SIT estimates from HY-2B and the two CS-2 products in Table 4. The bias between the HY2B calibrated SIT estimates and the AWI CS-2 SIT products on MYI was larger than that on FYI, with biases of 0.06 m on MYI and 0.02 m on FYI. The STD and RMSE for the HY-2B calibrated SIT estimates against the AWI CS-2 products on MYI (STD: 0.65 m, RSME: 0.65 m) are also higher than those on FYI (STD: 0.52 m, RSME: 0.52 m). However, the bias, STD, and RMSE for the HY2B calibrated SIT estimates against the GSFC CS-2 SIT on FYI (bias:  $-0.41$  m, STD: 0.51 m, RMSE: 0.67 m) are larger than those on MYI (bias:  $-0.11$ , STD: 0.49 m, RMSE: 0.50 m). The MREs for the HY2B calibrated SIT estimates against the AWI and GSFC CS-2 SIT products on FYI (AWI: 0.46, GSFC: 0.34) are higher than those on MYI (AWI: 0.23, GSFC: 0.16).

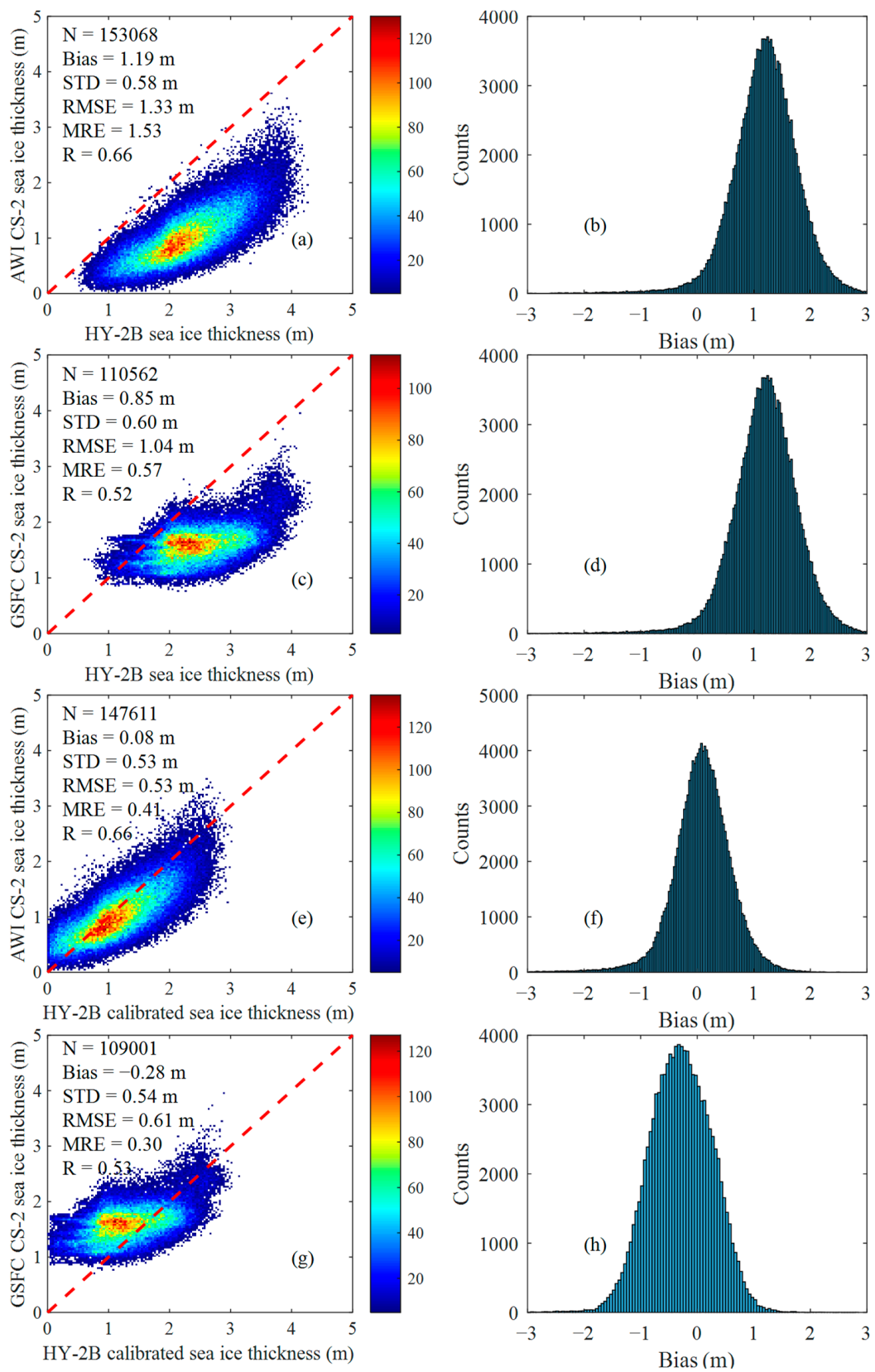


**Figure 9.** Comparison of the SIT estimates between the HY-2B and (a,b,e,f) AWI and (c,d,g,h) GSFC CS-2 SIT products.

**Table 3.** Bias between the SIT estimates from HY-2B and those from AWI and GSFC CS-2 SIT products in different SIT ranges.

		AWI CS-2					GSFC CS-2				
	SIT (m)	N	Bias (m)	STD (m)	RMSE (m)	MRE	N	Bias (m)	STD (m)	RMSE (m)	MRE
HY-2B	0–1	100,931	1.18	0.49	1.28	2.30	4178	0.92	0.59	1.09	1.05
	1–2	92,624	1.23	0.52	1.34	0.92	123,424	0.79	0.57	0.98	0.55
	2–3	16,694	0.92	0.65	1.12	0.43	25,403	0.75	0.61	0.97	0.35
	3–4	3020	0.09	0.77	0.77	0.17	2208	0.37	0.56	0.67	0.16
	4–5	642	−1.02	0.93	1.38	0.23	204	−0.57	0.80	0.98	0.15
	5–6	184	−2.37	1.08	2.61	0.43	27	−1.40	0.43	1.47	0.24
Calibrated HY-2B	0–1	100,931	0.08	0.44	0.45	0.68	4178	−0.19	0.52	0.55	0.50
	1–2	92,624	0.07	0.48	0.49	0.26	123,424	−0.34	0.52	0.62	0.33
	2–3	16,694	−0.29	0.60	0.67	0.18	25,403	−0.44	0.56	0.72	0.24
	3–4	3020	−1.12	0.72	1.34	0.31	2208	−0.86	0.53	1.01	0.23
	4–5	642	−2.22	0.87	2.39	0.50	204	−1.80	0.76	1.95	0.41
	5–6	184	−3.55	1.02	3.69	0.65	27	−2.64	0.41	2.67	0.48

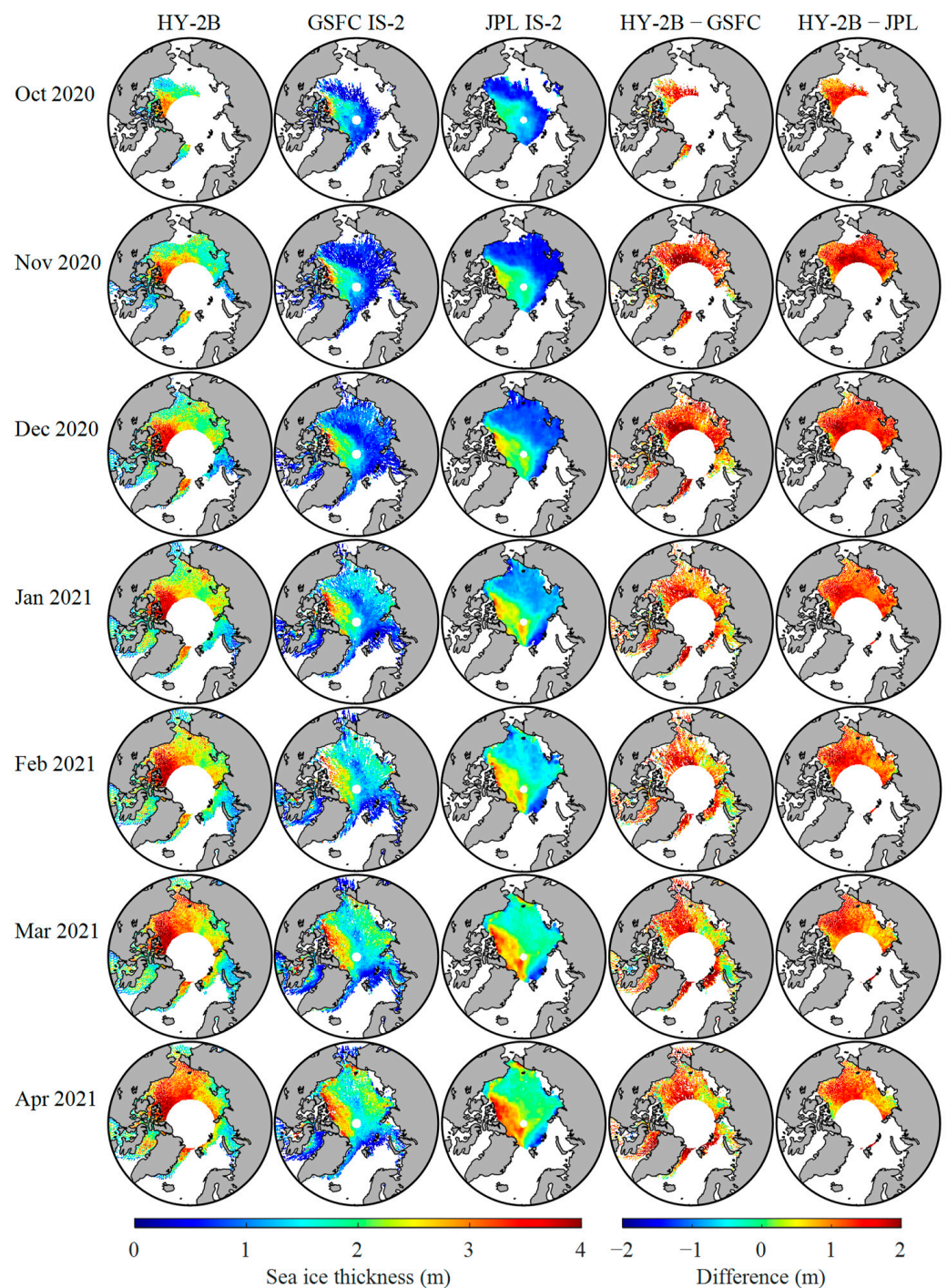
**Table 4.** Bias between the SIT estimates from HY-2B and those from AWI and GSFC CS-2 SIT products for different sea ice types.

		AWI CS-2					GSFC CS-2				
	Ice Type	N	Bias (m)	STD (m)	RMSE (m)	MRE	N	Bias (m)	STD (m)	RMSE (m)	MRE
HY-2B	FYI	167,298	1.14	0.55	1.27	1.57	120,528	0.73	0.57	0.92	0.51
	MYI	17,952	1.31	0.66	1.47	0.75	15,395	1.14	0.51	1.25	0.53
	ALL	185,250	1.16	0.56	1.29	1.49	135,923	0.77	0.58	0.97	0.51
Calibrated HY-2B	FYI	167,298	0.02	0.52	0.52	0.46	120,528	−0.41	0.51	0.67	0.34
	MYI	17,952	0.06	0.65	0.65	0.23	15,395	−0.11	0.49	0.50	0.16
	ALL	185,250	0.02	0.53	0.53	0.44	135,923	−0.37	0.54	0.65	0.32

### 3.2. Comparison against the IS-2 SIT Data

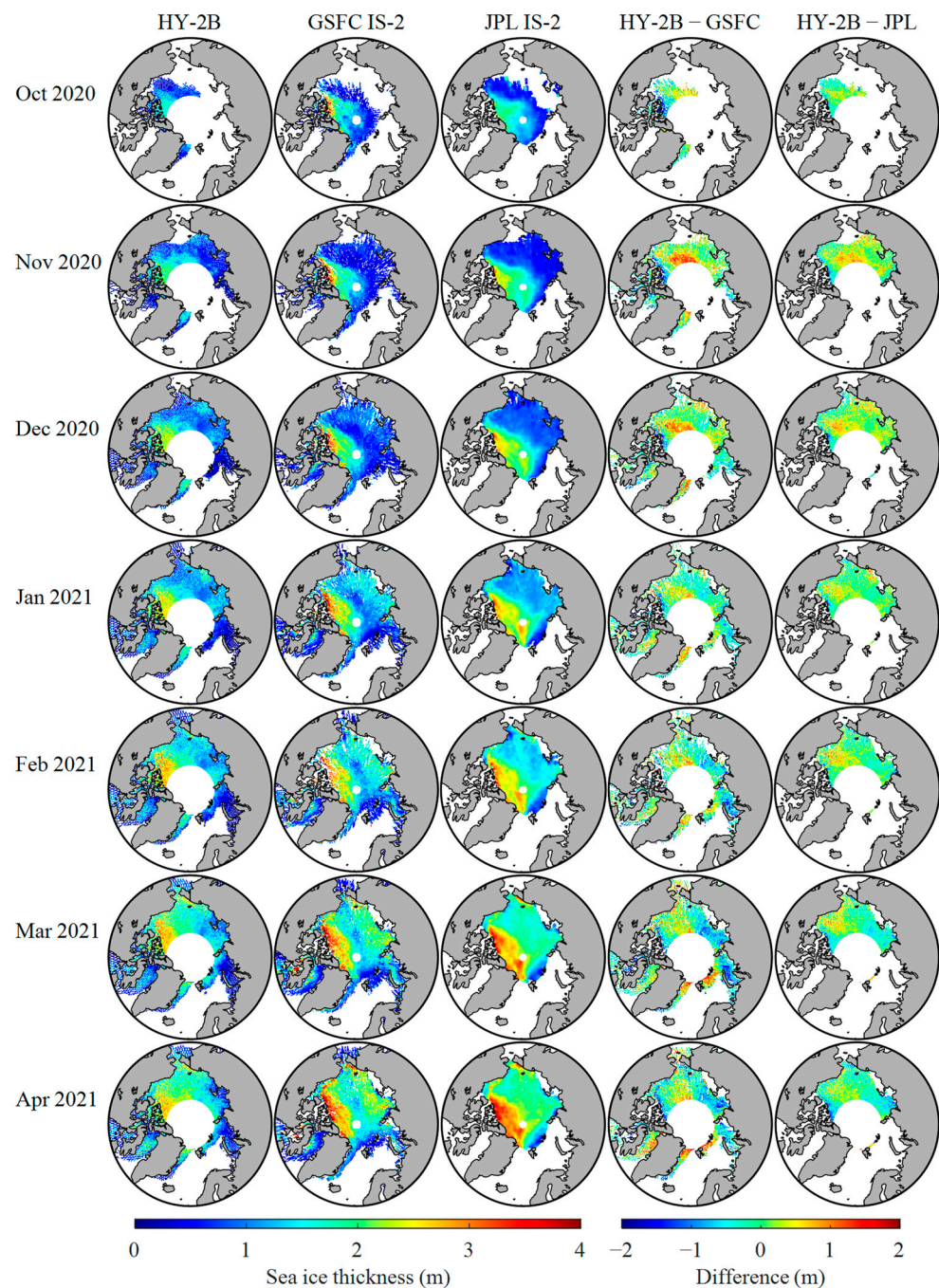
Figure 10 shows the monthly HY-2B estimates and the two (JPL and GSFC) IS-2 products, as well as the biases between the HY-2B estimates and the two IS-2 products for the 2020–2021 winter season. Similar to the results in Figures 7 and 8, Figure 11 shows the results for the HY-2B calibrated SIT estimates. Compared to the JPL and GSFC IS-2 SIT products, the HY-2B SIT estimates have positive biases in all months. After calibration, the HY-2B SIT estimates have relatively consistent results with the JPL and GSFC IS-2 SIT products.

We compared the SIT estimates from the radar altimetry data (HY-2B and CS-2) with those from the IS-2 laser altimetry data. To compare with the HY-2B estimates, we only used the CS-2 and IS-2 estimates with latitudes lower than 80.6°. When compared against the JPL IS-2 SIT products, the data from January 2019 to April 2021 were used, and the results are shown in Figure 12. Compared to the JPL IS-2 products, the HY-2B SIT estimates have an RMSE of 1.24 m, with a positive bias of 1.15 m, and an MRE of 1.01. After calibration, the RSME for the HY-2B estimates is reduced to 0.43 m with almost no bias (−0.01 m), which is very close to the results for AWI (RMSE: 0.42 m, bias: −0.20 m) and GSFC (RSME: 0.50 m, bias: 0.18 m) CS-2 products. The correlation coefficient for the HY-2B calibrated SIT estimates is 0.78, which is slightly higher than that for the GSFC CS-2 products (0.72) and lower than that for the AWI CS-2 products (0.84). The MRE for the HY-2B calibrated SIT estimates (0.22) is lower than that for the GSFC CS-2 products (0.32) and slightly higher than that for the AWI CS-2 products (0.20).



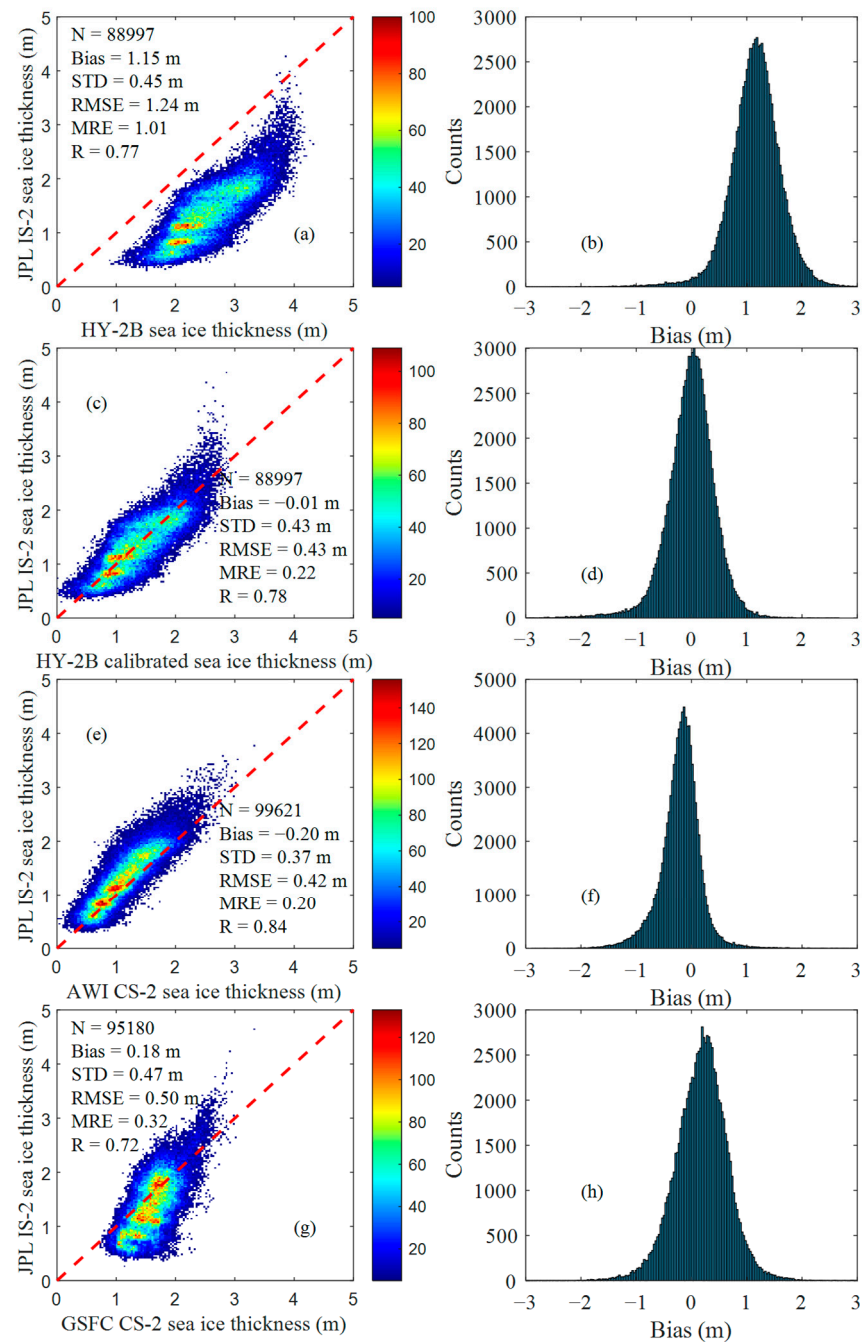
**Figure 10.** Comparison of the HY-2B SIT, GSFC IS-2 SIT, JPL IS-2 SIT, HY-2B SIT minus GSFC IS-2 SIT and JPL IS-2 SIT from October 2020 to April 2021.

Figure 13 shows the results for comparison against the GSFC IS-2 SIT products. Data from January 2019 to April 2022 were used. After calibration, the RMSE for the HY-2B SIT estimates is reduced from 1.25 m to 0.66 m, and the bias and MRE are also significantly reduced (bias: from 1.04 m to  $-0.09$  m, MRE: from 1.63 to 0.59). The RMSE, bias, and MRE for the AWI CS-2 products are respectively 0.63 m,  $-0.15$  m, and 0.54, which are close to the results of the HY-2B calibrated SIT estimates. The RMSE (0.71 m), bias (0.28 m), and MRE (0.86 m) for the GSFC CS-2 products are slightly higher than the values for the HY-2B calibrated SIT estimates. The correlation coefficients for the HY-2B (0.62), AWI CS-2 (0.65), and GSFC CS-2 (0.60) SIT estimates are close to each other.



**Figure 11.** Comparison of the HY-2B calibrated SIT, GSFC IS-2 SIT, JPL IS-2 SIT, HY-2B calibrated SIT minus GSFC IS-2 SIT, and JPL IS-2 SIT from October 2020 to April 2021.

We allocated the biases between the HY-2B SIT estimates and the two IS-2 products into six SIT ranges. Table 5 shows the statistics of the biases in different SIT ranges for the radar (HY-2B and CS-2) SIT estimates versus the two IS-2 SIT products. After calibration, the biases between the HY-2B SIT estimates and the two IS-2 SIT products are lowest (JPL: 0.006 m, GSFC:  $-0.13$  m) when SIT is larger than 1 m and smaller than 2 m. The biases increase with SIT when SIT is greater than 1 m. The STD and RMSE for the HY-2B calibrated SIT estimates increase with SIT when compared against both the JPL and GSFC IS-2 SIT products. Similar to the results for the HY-2B calibrated SIT estimates, the STDs and RMSEs for the AWI and GSFC CS-2 SIT products also increase with SIT when compared against the IS-2 SIT products. When SIT is higher than 3 m, the HY-2B calibrated SIT estimates significantly underestimate the SIT compared with the JPL and GSFC IS-2 SIT products.



**Figure 12.** Comparison of the SIT estimates between JPL IS-2 and (a,b) HY-2B, (c,d) HY-2B calibrated, (e,f) AWI CS-2, and (g,h) GSFC CS-2 SIT products.

Table 6 lists the biases in FYI, MYI, and total sea ice between the monthly average SIT estimates from the radar altimetry data (HY-2B and CS-2) and the JPL and GSFC IS-2 SIT products. The biases between the HY2B calibrated SIT estimates and the IS-2 SIT products on MYI (JPL:  $-0.25$  m, GSFC:  $-0.41$  m) are larger than those on FYI (JPL:  $0.02$  m, GSFC:  $-0.06$  m). The RMSEs for the HY2B calibrated SIT estimates on MYI (JPL:  $0.69$  m, GSFC:  $0.94$  m) are larger than those on FYI (JPL:  $0.37$  m, GSFC:  $0.63$  m). The MREs for the HY-2B calibrated SIT estimates on FYI (JPL:  $0.20$ , GSFC:  $0.53$ ) are higher than those on MYI (JPL:  $0.18$ , GSFC:  $0.27$ ). The RSMERs for the AWI and GSFC CS-2 SIT products on MYI are also slightly higher than those on FYI.

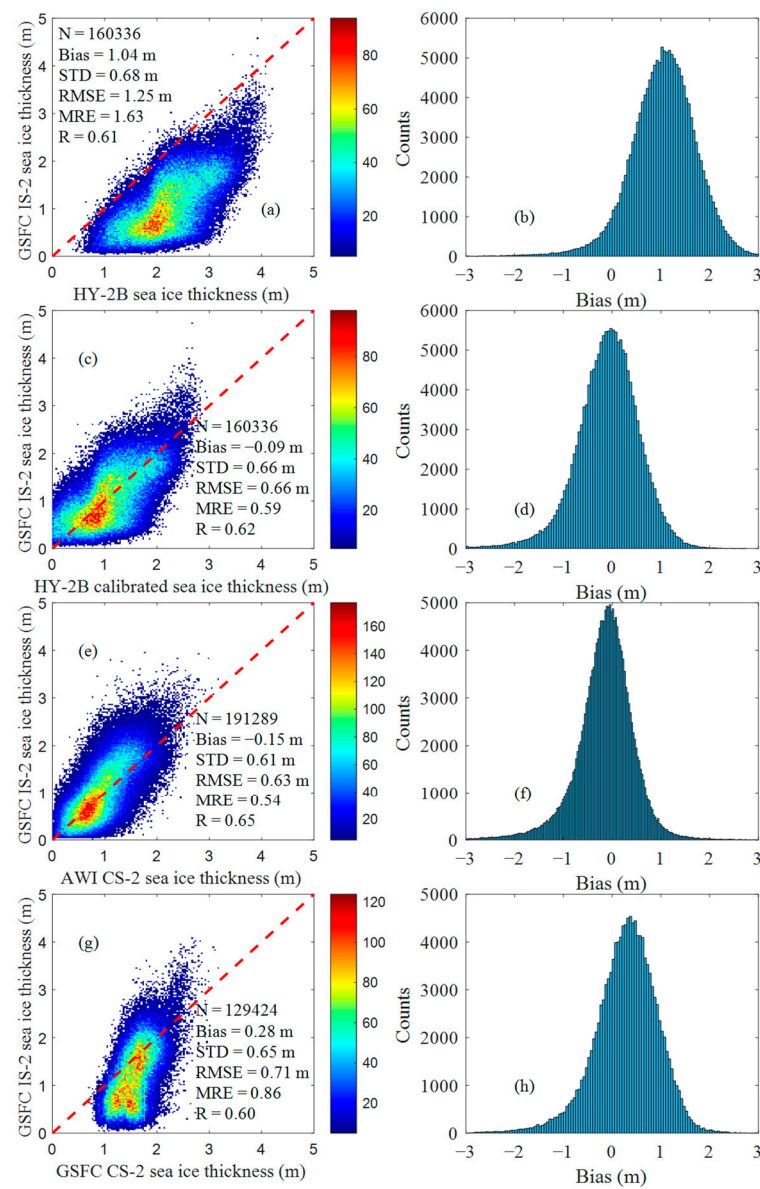


**Figure 13.** Comparison of the SIT estimates between GSFC IS-2 and (a,b) HY-2B, (c,d) HY-2B calibrated, (e,f) AWI CS-2, and (g,h) GSFC CS-2 SIT products.

**Table 5.** Bias between the SIT estimates from radar altimetry data and those from JPL and GSFC IS-2 SIT products in different SIT ranges.

	JPL IS-2						GSFC IS-2				
	SIT (m)	N	Bias (m)	STD (m)	RMSE (m)	MRE	N	Bias (m)	STD (m)	RMSE (m)	MRE
HY-2B	0–1	23,819	1.31	0.38	1.37	1.90	71,875	1.29	0.57	1.42	2.94
	1–2	49,665	1.17	0.40	1.23	0.81	64,091	1.01	0.56	1.16	0.73
	2–3	12,319	1.04	0.41	1.12	0.45	18,225	0.60	0.63	0.87	0.31
	3–4	2413	0.39	0.40	0.56	0.14	4455	0.009	0.70	0.70	0.15
	4–5	667	-0.45	0.37	0.58	0.10	1202	-0.83	0.69	1.08	0.18
	5–6	109	-1.19	0.32	1.24	0.22	316	-1.83	0.80	2.00	0.33

Table 5. Cont.

		JPL IS-2					GSFC IS-2				
	SIT (m)	N	Bias (m)	STD (m)	RMSE (m)	MRE	N	Bias (m)	STD (m)	RMSE (m)	MRE
Calibrated HY-2B	0-1	23,819	0.17	0.33	0.37	0.39	71,875	0.18	0.52	0.55	0.97
	1-2	49,665	0.006	0.36	0.36	0.18	64,091	-0.13	0.51	0.53	0.28
	2-3	12,319	-0.17	0.39	0.43	0.13	18,225	-0.58	0.58	0.83	0.27
	3-4	2413	-0.84	0.39	0.92	0.24	4455	-1.22	0.66	1.39	0.34
	4-5	667	-1.69	0.35	1.73	0.38	1202	-2.07	0.66	2.17	0.46
	5-6	109	-2.44	0.30	2.46	0.46	316	-3.06	0.76	3.15	0.56
AWI CS-2	0-1	27,528	0.01	0.34	0.34	0.25	91,094	0.16	0.44	0.47	0.83
	1-2	55,201	-0.21	0.30	0.37	0.18	73,756	-0.24	0.46	0.52	0.26
	2-3	13,687	-0.45	0.44	0.63	0.21	20,742	-0.76	0.58	0.96	0.33
	3-4	2521	-0.67	0.50	0.84	0.20	5087	-1.35	0.84	1.60	0.40
	4-5	684	-0.79	0.64	1.02	0.20	1391	-1.95	1.12	2.25	0.44
	5-6	107	-0.78	0.81	1.13	0.18	355	-2.55	1.36	2.89	0.48
GSFC CS-2	0-1	23,265	0.61	0.34	0.70	0.84	50,339	0.80	0.38	0.89	1.89
	1-2	54,951	0.17	0.33	0.37	0.20	56,514	0.17	0.35	0.40	0.20
	2-3	13,633	-0.29	0.33	0.44	0.15	16,990	-0.42	0.41	0.58	0.20
	3-4	2534	-0.64	0.43	0.77	0.19	4066	-1.00	0.51	1.12	0.29
	4-5	680	-0.98	0.47	1.09	0.22	1086	-1.65	0.66	1.78	0.37
	5-6	109	-1.25	0.62	1.40	0.24	264	-2.21	0.71	2.32	0.41

Table 6. Bias between the SIT estimates from radar altimetry data and those from JPL and GSFC IS-2 SIT products for different sea ice types.

		JPL IS-2					GSFC IS-2				
	Ice Type	N	Bias (m)	STD (m)	RMSE (m)	MRE	N	Bias (m)	STD (m)	RMSE (m)	MRE
HY-2B	FYI	66,997	1.17	0.40	1.24	1.08	127,298	1.06	0.65	1.24	1.69
	MYI	11,067	0.99	0.65	1.19	0.52	12,254	0.84	0.84	1.19	0.59
	ALL	78,064	1.15	0.44	1.23	1.00	139,552	1.04	0.67	1.24	1.59
Calibrated HY-2B	FYI	66,997	0.02	0.37	0.37	0.23	127,298	-0.06	0.62	0.63	0.59
	MYI	11,067	-0.25	0.64	0.69	0.18	12,254	-0.41	0.84	0.94	0.27
	ALL	78,064	-0.01	0.43	0.43	0.22	139,552	-0.09	0.65	0.66	0.57
AWI CS-2	FYI	75,838	-0.17	0.34	0.38	0.20	159,465	-0.12	0.60	0.61	0.53
	MYI	11,602	-0.39	0.44	0.59	0.18	12,822	-0.53	0.75	0.92	0.27
	ALL	87,440	-0.20	0.36	0.41	0.19	172,287	-0.15	0.62	0.64	0.51
GSFC CS-2	FYI	71,935	0.25	0.43	0.50	0.36	103,639	0.37	0.57	0.68	0.91
	MYI	11,583	-0.21	0.45	0.50	0.14	12,015	-0.35	0.76	0.84	0.25
	ALL	83,518	0.19	0.46	0.50	0.32	115,654	0.29	0.64	0.70	0.85

### 3.3. Comparison against the OIB Ice Thickness Data

We compared the HY-2B SIT estimates with the OIB airborne observation data, and the results are shown in Figure 14. Because the HY-2B radar altimeter can only cover the 80.6° N/S region, only seventeen grids could be evaluated when overlapped with the OIB airborne data collected in April 2019. The correlation coefficient between the HY-2B SIT estimates and the OIB SIT measurements was 0.89, the RMSE is 1.31 m, the mean bias is 0.13 m, and the MRE is 0.65. However, after calibration, the RSME (1.72 m) and bias (-1.08 m) are increased while the MRE is reduced (0.53). As shown in Tables 3 and 5, the HY-2B calibrated SIT estimates underestimate the SIT at high SIT values (SIT is higher than 3 m). As shown in Figure 14, about half the OIB SIT values are higher than 3 m. Therefore, the RMSE of HY-2B compared with OIB after calibration is larger than before calibration. The linear calibration model is not suitable for all SIT ranges. The linear calibration model

is not suitable for all SIT ranges. When only the measurements of the OIB SIT value less than 4 m (9 points) are used to calculate the results, the bias ( $-0.02$  m), RMSE (0.92 m), and MRE (1.07 m) for the HY-2B calibrated SIT estimates are significantly reduced compared with the ones without calibration (bias: 1.17 m, RMSE: 1.49 m, MRE: 1.91).

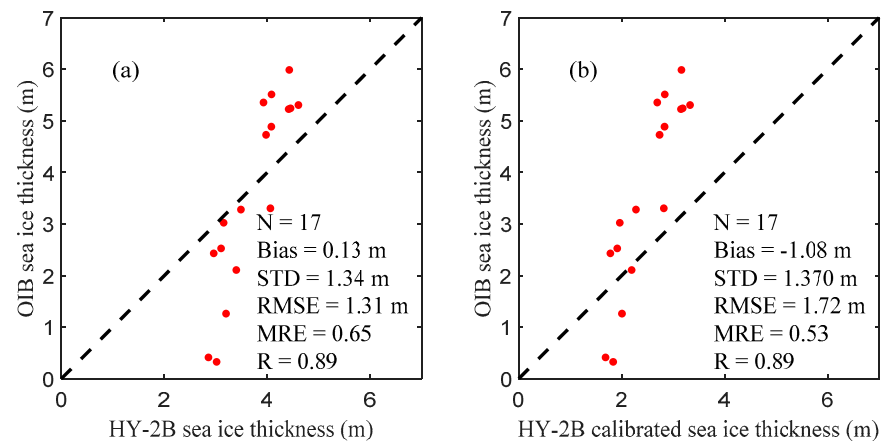


**Figure 14.** Comparison of the SIT estimates between OIB and (a) HY-2B and (b) HY-2B calibrated SIT products.

Figure 15 shows the comparison of the CS-2 and IS-2 SIT products with the OIB data. The left column uses all the data up to  $88^{\circ}\text{N}$ , while the right column only uses data below  $80.6^{\circ}\text{N}$ . When all latitude data are used, the RMSE is 0.84 m for the AWI CS-2 products, 0.76 m for the GSFC CS-2 products, 0.56 m for the JPL IS-2 products, and 1.01 m for the GSFC IS-2 products. The JPL IS-2 SIT products have the highest correlation coefficient (0.75), and the GSFC CS-2 SIT products have the lowest bias ( $-0.09$  m) among the four products. When only data with a latitude less than  $80.6^{\circ}\text{N}$  is used, the AWI CS-2 SIT products have the highest correlation coefficient (0.81) and the JPL IS-2 SIT products have the lowest RMSE (0.46 m).

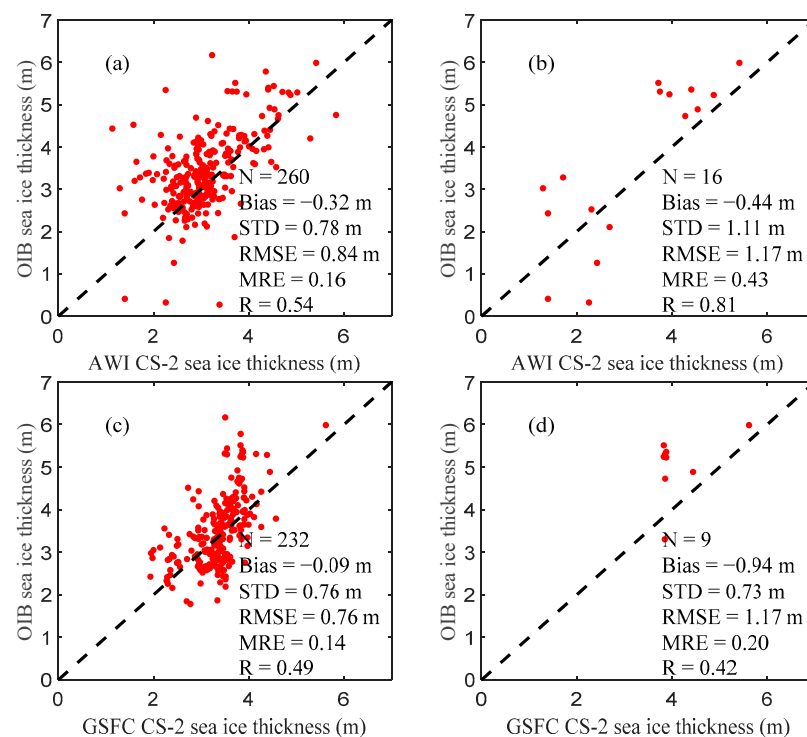


**Figure 15.** Cont.

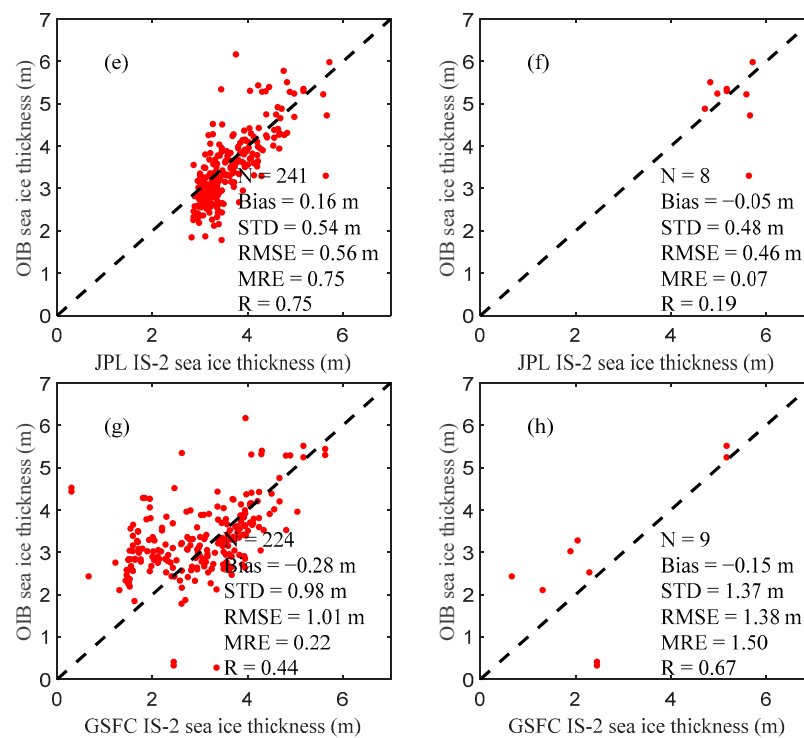


**Figure 15.** Comparison of the SIT estimates between OIB and (a,b) AWI CS-2, (c,d) GSFC CS-2, (e,f) JPL IS-2, and (g,h) GSFC IS-2 SIT products.

### 3.4. Comparison against the BGEP Ice Draft Data

We computed the SIT estimates using the BGEP ice draft data and then compared them with the SIT estimates from the altimetry data. We computed the BGEP equivalent SIT estimates using [8]:

$$h_i = \frac{h_{draft}\rho_w - h_s\rho_s}{\rho_i} \quad (14)$$

where  $h_i$  is the SIT,  $h_{draft}$  is the BGEP ice draft,  $h_s$  is the snow depth,  $\rho_w$  is seawater density,  $\rho_s$  is the snow density, and  $\rho_i$  is sea ice density. Monthly averages of the SIT estimates derived from the altimetry data were then taken within 100 km of each BGEP mooring and compared with monthly averages of SIT obtained by each mooring.

Figure 16 shows the comparison of the BGEP SIT estimates with the SIT estimates derived from the altimetry data. The mean bias, STD, RMSE, MRE, and correlation coefficient for the HY-2B SIT estimates are 1.61 m, 0.29 m, 1.64 m, 1.72 and 0.84, respectively. After calibration, the mean bias (0.42 m), RMSE (0.50 m), and MRE (0.49) are significantly reduced. The correlation coefficient is 0.86 for the AWI CS-2 products, 0.79 for the GSFC CS-2 products, 0.93 for the GSFC IS-2 products, and 0.97 for the JPL IS-2 products. The JLP IS-2 data have the lowest RMSE (0.18 m) and MRE (0.19) among the six data sets.

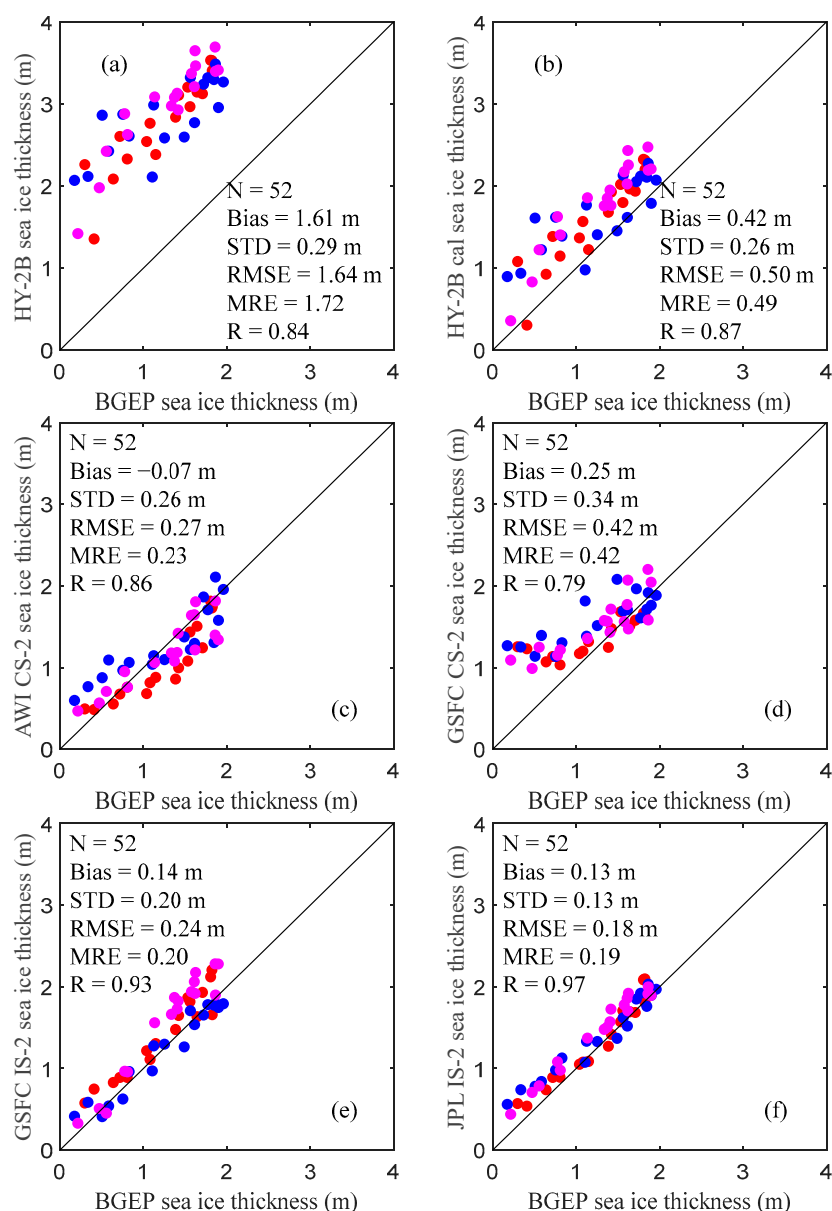


**Figure 16.** Comparison of the SIT estimates between BGEP and (a) HY-2B, (b) HY-2B calibrated, (c) AWI CS-2, (d) GSFC CS-2, (e) GSFC IS-2 and (f) JPL IS-2. Blue, red, and purple represent the mooring A, B, and D, respectively.

#### 4. Discussion

We validated the HY-2B SIT estimates using CS-2 SIT products, IS-2 SIT products, OIB SIT data, and the BGEP ice draft data. In this section, we analyzed the monthly variations of the HY-2B SIT estimates. The monthly average Arctic SIT estimates from January 2019 to April 2022 are computed and shown in Figure 17. To compare with the HY-2B SIT estimates, we only used the data below  $80.6^{\circ}\text{N}$  for the CS-2 and IS-2 SIT products. Similar to the CS-2 and IS-2 SIT products, the HY-2B SIT estimates have obvious seasonal variations. In the Arctic sea ice growth season, the mean HY-2B SIT estimate is the lowest in October and increases month by month, reaching the maximum in April of the next year. The growth rate of the mean SIT in each sea ice growth season from 2019 to 2022 was computed and shown in Table 7. The JPL IS-2 SIT products have higher growth rates than other products because they have no data in Baffin Bay, the Kara Sea, or the Canadian Arctic Archipelago. The growth rates in MYI are higher than those in FYI on the whole. The total growth rate

of the HY-2B calibrated SIT estimates is close to those of the AWI CS-2, GSFC CS-2, and GSFC IS-2 SIT products.

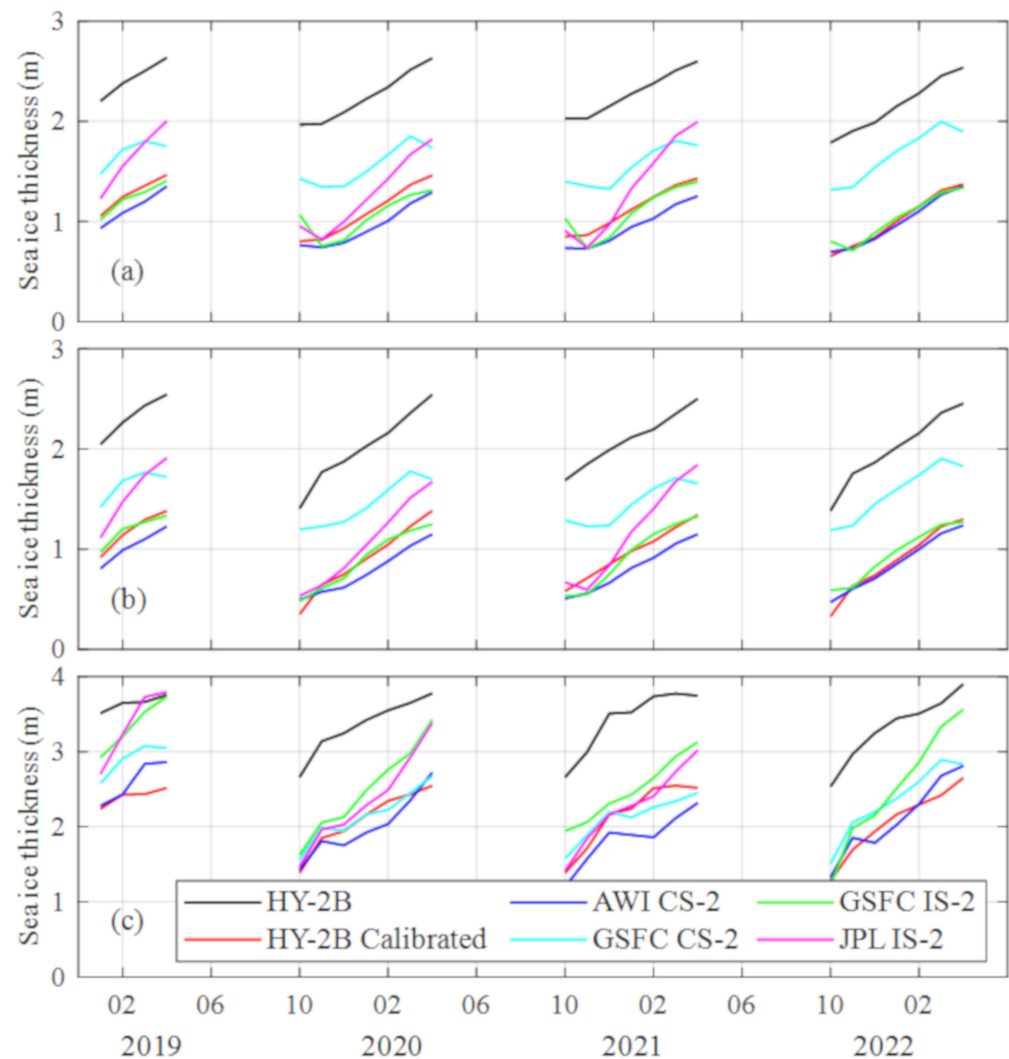


**Figure 17.** Variations in the monthly average Arctic SIT from January 2019 to April 2022. (a) Total first-year and multiyear SIT. (b) first-year, and (c) multiyear SIT.

**Table 7.** SIT growth rate ( $\text{m month}^{-1}$ ) in each growth season from 2019 to 2022.

Time Span	Ice Type	HY2B	Calibrated HY-2B	AWI CS-2	GSFC CS-2	GSFC IS-2	JPL IS-2
October 2019–April 2020	FYI	0.17	0.16	0.11	0.10	0.14	0.20
	MYI	0.17	0.18	0.19	0.16	0.28	0.29
	ALL	0.11	0.12	0.10	0.08	0.07	0.17
October 2020–April 2021	FYI	0.13	0.13	0.11	0.09	0.15	0.22
	MYI	0.18	0.19	0.16	0.13	0.20	0.24
	ALL	0.10	0.11	0.10	0.08	0.10	0.22
October 2021–April 2022	FYI	0.17	0.16	0.13	0.13	0.13	-
	MYI	0.20	0.21	0.24	0.22	0.37	-
	ALL	0.13	0.13	0.12	0.12	0.11	-

## 5. Conclusions

The HY-2B radar altimeter can provide data up to  $80.6^\circ$  latitude and can be used to retrieve the Arctic sea ice thickness. In this study, we processed the HY-2B radar altimetry

data from January 2019 to April 2022. The TFMRA retracker was used to process the HY-2B radar altimeter waveforms. The range and geophysical corrections were computed and added to the altimeter-derived range. The processed HY-2B radar altimetry data were used to retrieve the Arctic SIT values.

We first used the AWI and GSFC CS-2 SIT products to validate the HY-2B SIT estimates. Compared to the AWI CS-2 SIT products, the HY-2B SIT estimates have a bias of more than 1 m, and the MRE is larger than 1. We used a linear regression method to calibrate the HY-2B SIT estimates. After calibration, the bias, RMSE, and MRE for the HY-2B SIT estimates have been significantly reduced. Compared to the AWI CS-2 SIT products, the HY-2B calibrated SIT estimates have an RMSE of 0.53 m, a bias of 0.08 m, and an MRE of 0.41. The HY-2B calibrated SIT estimates and the AWI CS-2 SIT estimates have relatively consistent spatial distributions.

We then compared the HY-2B SIT estimates with the JPL and GSFC IS-2 SIT products. Compared to the JPL IS-2 SIT products, the RMSE and correlation coefficient for the HY-2B calibrated SIT estimates are 0.43 m and 0.78, respectively. The HY-2B calibrated SIT estimates underestimate the SIT at high SIT values (SIT is higher than 3 m). The biases for the HY-2B calibrated SIT estimates increase with SIT when SIT is greater than 1 m. The STD and RMSE for the HY-2B calibrated SIT estimates increase with SIT when compared against both the JPL and GSFC IS-2 SIT products.

We also used the OIB ice thickness data to validate the HY-2B SIT estimates. A comparison with the OIB SIT values obtained in April 2019 shows that the correlation coefficient between the HY-2B calibrated SIT estimates and OIB values is 0.89 and the RMSE is 1.72 m. In addition, we used the BGEP SIT estimates derived from the ice draft data to validate the HY-2B products. The RMSE and correlation coefficient for the HY-2B calibrated SIT estimates are 0.50 m and 0.87, respectively.

Finally, we analyzed the monthly variations of the HY-2B SIT estimates. The total growth rate of the HY-2B calibrated SIT estimates is close to those of the AWI CS-2, GSFC CS-2, and GSFC IS-2 SIT products. The growth rates in MYI are higher than those in FYI on the whole.

The linear regression method used to calibrate the HY-2B SIT estimates can significantly reduce the bias, RMSE, and MRE for the HY-2B SIT estimates compared with the CS-2 and IS-2 SIT products and the BGEP SIT measurements when SIT is lower than 3 m. More than 95% of the SIT values are lower than 3 m when the latitude is lower than 80.6°N. Therefore, the HY-2B calibrated SIT estimates in this study are reliable. The HY-2B altimetry data is a possible source for sea ice thickness data at lower latitudes and will help us better understand the sea ice response to climate change. In the future, we will develop new calibration methods suitable for all SIT ranges.

In this study, we did not accurately identify sea ice leads and floes when calculating the sea ice freeboard. The sea ice leads and floes are usually identified using the altimeter waveform parameters such as pulse peakiness, backscattering coefficient, and stack standard deviation [8]. In the future, we will develop a more accurate classification algorithm to identify sea ice leads and floes and use it to estimate the sea ice freeboard and sea ice thickness.

**Author Contributions:** Conceptualization, M.J., W.Z. and K.X.; methodology, M.J., W.Z. and K.X.; software, M.J.; formal analysis, M.J. and W.Z.; investigation, M.J. and W.Z.; data curation, M.J. and Y.J.; writing—original draft preparation, M.J.; writing—review and editing, W.Z., M.J., K.X. and Y.J.; project administration, M.J. and K.X.; funding acquisition, M.J. and Y.J. All authors have read and agreed to the published version of the manuscript.

**Funding:** This research was funded by the National Natural Science Foundation of China (Grant No. 41906199), the Foundation of Key Laboratory of Space Ocean Remote Sensing and Application, MNR (No. E0C01kA340), and the Youth Innovation Project of National Space Science Center of Chinese Academy of Sciences (No. EOPD40012S).

**Data Availability Statement:** The HY-2B L1 data were downloaded from the NSOAS, available online at <https://osdds.nsoas.org.cn/> (accessed on 29 October 2022). The AWI CS-2 SIT products were downloaded from AWI, available online at [ftp://ftp.awi.de/sea\\_ice/product/cryosat2/v2p5/nh/l3\\_c\\_grid/month/](ftp://ftp.awi.de/sea_ice/product/cryosat2/v2p5/nh/l3_c_grid/month/) (accessed on 11 October 2022). The GSFC CS-2 SIT products were downloaded from NSIDC, and available online at <https://nsidc.org/data/RDEFT4/versions/1> (accessed on 11 October 2022). The GSFC IS-2 SIT products were downloaded from NSIDC, and available online at <https://nsidc.org/data/is2sitmogr4/versions/2> (accessed on 11 October 2022). The JPL IS-2 Arctic monthly average SIT products are available online at <https://icesat-2.gsfc.nasa.gov/sea-ice-data/kacimi-kwok-2022> (Kacimi et al., 2022) (last access: 30 June 2022). The IceBridge L4-level data (IDCS14) are downloaded from NSIDC, and available online at <https://nsidc.org/data/NSIDC-0708/versions/1/> (accessed on 11 October 2022). The sea ice concentration and sea ice type data were downloaded from OSI-SAF, and available online at <https://osi-saf.eumetsat.int> (accessed on 11 October 2022). The DTU21 MSS data are downloaded from DTU, and available online at <ftp://ftp.space.dtu.dk/pub/> (accessed on 11 October 2022). The BGEP sea ice draft data were downloaded from the BGEP website, and available online at <https://www2.whoi.edu/site/beaufortgyre/data/mooring-data/2018-2021-mooring-data-from-the-bgep-project/> (accessed on 11 October 2022). The NCEP FNL Operational Global Analysis data were downloaded from NCEP, and available online at <https://rda.ucar.edu/datasets/ds083.2/> (accessed on 11 October 2022). The JPL-GIM TEC data were downloaded from Ionospheric and Precision Positioning Group, Academy of Aerospace Information (GIPP/AIR), Chinese Academy of Sciences, available online at <ftp://ftp.gipp.org.cn/product/ionex/> (accessed on 11 October 2022). The FES2014 ocean tide model data and the MOG2D DAC data were downloaded from AVISO, and available online at <https://www.aviso.altimetry.fr/en/data.html> (accessed on 11 October 2022). The earth orientation data used were downloaded from IERS, and available online at <https://www.iers.org/IERS/EN/DataProducts/EarthOrientationData/eop.html> (accessed on 29 October 2022).

**Acknowledgments:** The authors thank NSOAS for the HY-2B altimetry data, AWI for the CS-2 SIT data, JPL for the IS-2 SIT data, NSIDC for the IS-2, CS-2 SIT data, and OIB airborne data, BGEP for the sea ice draft data, OSI-SAF for the sea ice concentration and sea ice type data, DTU for the DTU21 MSS data, NCEP for the surface pressure data and total column water vapor data, GIPP/AIR for the TEC data, AVISO for the DAC and FES2014 ocean tide model data and IERS for the earth orientation data.

**Conflicts of Interest:** The authors declare no conflict of interest.

## References

1. Toggweiler, J.R.; Russell, J. Ocean circulation in a warming climate. *Nature* **2008**, *451*, 286–288. [[CrossRef](#)] [[PubMed](#)]
2. Dickson, B. Oceanography: All change in the Arctic. *Nature* **1999**, *397*, 389–391. [[CrossRef](#)] [[PubMed](#)]
3. Holland, M.M.; Bitz, C.M.; Tremblay, B. Future abrupt reductions in the summer Arctic sea ice. *Geophys. Res. Lett.* **2006**, *33*, 265–288. [[CrossRef](#)]
4. Laxon, S.; Peacock, N.; Smith, D. High interannual variability of sea ice thickness in the Arctic region. *Nature* **2003**, *425*, 947–950. [[CrossRef](#)] [[PubMed](#)]
5. Guerreiro, K.; Fleury, S.; Zakharova, E.; Kouraev, A.; Rémy, F.; Maisongrande, P. Comparison of CryoSat-2 and ENVISAT radar freeboard over Arctic sea ice: Toward an improved Envisat freeboard retrieval. *Cryosphere* **2017**, *11*, 2059–2073. [[CrossRef](#)]
6. Paul, S.; Hendricks, S.; Ricker, R.; Kern, S.; Rinne, E. Empirical parametrization of Envisat freeboard retrieval of Arctic and Antarctic sea ice based on CryoSat-2: Progress in the ESA Climate Change Initiative. *Cryosphere* **2018**, *12*, 2437–2460. [[CrossRef](#)]
7. Kwok, R.; Cunningham, G.F. Variability of Arctic sea ice thickness and volume from CryoSat-2. *Philos. Trans. A Math. Phys. Eng. Sci.* **2015**, *373*, 20140157. [[CrossRef](#)]
8. Tilling, R.L.; Ridout, A.; Shepherd, A. Estimating Arctic sea ice thickness and volume using CryoSat-2 radar altimeter data. *Adv. Space Res.* **2018**, *62*, 1203–1225. [[CrossRef](#)]
9. Lawrence, I.R.; Armitage, T.W.K.; Tsamados, M.C.; Stroeve, J.C.; Dinardo, S.; Ridout, A.L.; Muir, A.; Tilling, R.L.; Shepherd, A. Extending the Arctic sea ice freeboard and sea level record with the Sentinel-3 radar altimeters. *Adv. Space Res.* **2021**, *68*, 711–723. [[CrossRef](#)]
10. Kwok, R.; Cunningham, G.F. ICESat over Arctic sea ice: Estimation of snow depth and ice thickness. *J. Geophys. Res.* **2008**, *113*, C08010. [[CrossRef](#)]
11. Kurtz, N.T.; Markus, T.; Cavalieri, D.J.; Sparling, L.C.; Krabill, W.B.; Gasiewski, A.J.; Sonntag, J.G. Estimation of sea ice thickness distributions through the combination of snow depth and satellite laser altimetry data. *J. Geophys. Res.* **2009**, *114*, C10007. [[CrossRef](#)]

12. Farrell, S.L.; Laxon, S.W.; McAdoo, D.C.; Yi, D.; Zwally, H.J. Five years of Arctic sea ice freeboard measurements from the Ice, Cloud and land Elevation Satellite. *J. Geophys. Res.* **2009**, *114*, C04008. [[CrossRef](#)]
13. Petty, A.A.; Kurtz, N.T.; Kwok, R.; Markus, T.; Neumann, T.A. Winter Arctic Sea Ice Thickness from ICESat-2 Freeboards. *J. Geophys. Res. Ocean.* **2020**, *125*, e2019JC015764. [[CrossRef](#)]
14. Petty, A.A.; Keeney, N.; Cabaj, A.; Kushner, P.; Bagnardi, M. Winter Arctic sea ice thickness from ICESat-2: Upgrades to freeboard and snow loading estimates and an assessment of the first three winters of data collection. *Cryosphere* **2023**, *17*, 127–156. [[CrossRef](#)]
15. Jiang, M.; Xu, K.; Jia, Y.; Fan, C.; Xu, X. Evaluation of HY-2B Altimeter Products Over Ocean. In Proceedings of the IGARSS 2020—2020 IEEE International Geoscience and Remote Sensing Symposium, Waikoloa, HI, USA, 26 September–2 October 2020; pp. 5858–5861. [[CrossRef](#)]
16. Xu, K.; Liu, P.; Tang, Y.; Yu, X. The improved design for HY-2B radar altimeter. In Proceedings of the IGARSS 2020—2020 IEEE International Geoscience and Remote Sensing Symposium, Fort Worth, TX, USA, 23–28 July 2017. [[CrossRef](#)]
17. Philip, A.; Taburet, G.; Charles, E.; Raynal, M.; Faugère, Y.; Quérue, N.; Bignalet-Cazalet, F.; Dibarboure, G. HY-2B Now Used Operationally in Multi-Mission Sea Level and Wave Systems. Available online: [https://ostst.avisio.altimetry.fr/fileadmin/user\\_upload/tx\\_ausyclsseminar/files/OSTST\\_2020\\_HY2B\\_feedbacks\\_and\\_contribution.pdf](https://ostst.avisio.altimetry.fr/fileadmin/user_upload/tx_ausyclsseminar/files/OSTST_2020_HY2B_feedbacks_and_contribution.pdf) (accessed on 14 February 2023).
18. Laxon, S.W.; Giles, K.A.; Ridout, A.L.; Wingham, D.J.; Willatt, R.; Cullen, R.; Kwok, R.; Schweiger, A.; Zhang, J.; Haas, C.; et al. CryoSat-2 estimates of Arctic sea ice thickness and volume. *Geophys. Res. Lett.* **2013**, *40*, 732–737. [[CrossRef](#)]
19. Kurtz, N.T.; Galin, N.; Studinger, M. An improved CryoSat-2 sea ice freeboard retrieval algorithm through the use of waveform fitting. *Cryosphere* **2014**, *8*, 1217–1237. [[CrossRef](#)]
20. Ricker, R.; Hendricks, S.; Helm, V.; Skourup, H.; Davidson, M. Sensitivity of CryoSat-2 Arctic sea-ice freeboard and thickness on radar-waveform interpretation. *Cryosphere* **2014**, *8*, 1607–1622. [[CrossRef](#)]
21. Markus, T.; Neumann, T.; Martino, A.; Abdalati, W.; Brunt, K.; Csatho, B.; Farrell, S.; Fricker, H.; Gardner, A.; Harding, D.; et al. The Ice, Cloud, and land Elevation Satellite-2 (ICESat-2): Science requirements, concept, and implementation. *Remote Sens. Environ.* **2017**, *190*, 260–273. [[CrossRef](#)]
22. Kacimi, S.; Kwok, R. Arctic Snow Depth, Ice Thickness, and Volume from ICESat-2 and CryoSat-2: 2018–2021. *Geophys. Res. Lett.* **2022**, *49*, e2021GL097448. [[CrossRef](#)]
23. Kwok, R.; Kacimi, S.; Webster, M.A.; Kurtz, N.T.; Petty, A.A. Arctic Snow Depth and Sea Ice Thickness from ICESat-2 and CryoSat-2 Freeboards: A First Examination. *J. Geophys. Res. Ocean.* **2020**, *125*, e2019JC016008. [[CrossRef](#)]
24. Kurtz, N.T.; Farrell, S.L.; Studinger, M.; Galin, N.; Harbeck, J.P.; Lindsay, R.; Onana, V.D.; Panzer, B.; Sonntag, J.G. Sea ice thickness, freeboard, and snow depth products from Operation IceBridge airborne data. *Cryosphere* **2013**, *7*, 1035–1056. [[CrossRef](#)]
25. Dawson, G.; Landy, J.; Tsamados, M.; Komarov, A.S.; Howell, S.; Heorton, H.; Krumpfen, T. A 10-year record of Arctic summer sea ice freeboard from CryoSat-2. *Remote Sens. Environ.* **2022**, *268*, 112744. [[CrossRef](#)]
26. Hendricks, S.; Ricker, R. Product User Guide & Algorithm Specification-AWI CryoSat-2 Sea Ice Thickness (Version 2.3). Available online: <https://www.researchgate.net/publication/346677382> (accessed on 14 February 2023).
27. Jiang, M.; Xu, K.; Zhong, W.; Jia, Y. Preliminary HY-2B Radar Freeboard Retrieval Over Arctic Sea Ice. In Proceedings of the IGARSS 2022—2022 IEEE International Geoscience and Remote Sensing Symposium, Kuala Lumpur, Malaysia, 17–22 July 2022; pp. 3904–3907. [[CrossRef](#)]
28. Helm, V.; Humbert, A.; Miller, H. Elevation and elevation change of Greenland and Antarctica derived from CryoSat-2. *Cryosphere* **2014**, *8*, 1539–1559. [[CrossRef](#)]
29. Fernandes, M.J.; Lázaro, C.; Vieira, T. On the role of the troposphere in satellite altimetry. *Remote Sens. Environ.* **2021**, *252*, 112149. [[CrossRef](#)]
30. Jiang, M.; Xu, K.; Liu, Y.; Zhao, J.; Wang, L. Assessment of reprocessed sea surface height measurements derived from HY-2A radar altimeter and its application to the observation of 2015–2016 El Niño. *Acta Oceanol. Sin.* **2018**, *37*, 115–129. [[CrossRef](#)]
31. Wu, Q.; Zhang, P.; Sun, M.; Liu, S.; Wang, H.; Chen, S. Performance evaluation of GIMs released by different IGS ionosphere associate analysis centers in ionospheric constrained single-frequency precise point positioning. *Adv. Space Res.* **2021**, *68*, 4834–4856. [[CrossRef](#)]
32. Lyard, F.H.; Allain, D.J.; Cancet, M.; Carrère, L.; Picot, N. FES2014 global ocean tide atlas: Design and performance. *Ocean. Sci.* **2021**, *17*, 615–649. [[CrossRef](#)]
33. Carrère, L.; Lyard, F. Modeling the barotropic response of the global ocean to atmospheric wind and pressure forcing-comparisons with observations. *Geophys. Res. Lett.* **2003**, *30*, 1275. [[CrossRef](#)]
34. Cartwright, D.E.; Edden, A.C. Corrected tables of tidal harmonics. *Geophys. J. Int.* **1973**, *33*, 253–264. [[CrossRef](#)]
35. Wahr, J.M. Deformation induced by polar motion. *J. Geophys. Res.* **1985**, *90*, 9363–9368. [[CrossRef](#)]
36. Andersen, O.B.; Abulaitjiang, A.; Zhang, S.; Rose, K.S. A New High Resolution Mean Sea Surface (DTU21MSS) for Improved Sea Level Monitoring. In Proceedings of the EGU General Assembly Conference Abstracts, Online, 19–30 April 2021; p. EGU21-16084. [[CrossRef](#)]
37. Kwok, R.; Cunningham, G.F.; Zwally, H.J.; Yi, D. Ice, Cloud, and land Elevation Satellite (ICESat) over Arctic sea ice: Retrieval of freeboard. *J. Geophys. Res.* **2007**, *112*, C12013. [[CrossRef](#)]
38. Lindsay, R.W.; Rothrock, D.A. Arctic sea ice leads from advanced very high resolution radiometer images. *J. Geophys. Res. Ocean* **1995**, *100*, 4533–4544. [[CrossRef](#)]

39. Zwally, H.J.; Yi, D.; Kwok, R.; Zhao, Y. ICESat measurements of sea ice freeboard and estimates of sea ice thickness in the Weddell Sea. *J. Geophys. Res.* **2008**, *113*, C02S15. [[CrossRef](#)]
40. Skourup, H.; Forsberg, R. Sea ice freeboards from ICESat—A comparison to airborne lidar measurements. In *Arctic Sea Ice Thickness: Past, Present and Future*; Springer: Berlin/Heidelberg, Germany, 2006; pp. 82–92.
41. Zhang, S.; Xuan, Y.; Li, J.; Geng, T.; Li, X.; Xiao, F. Arctic Sea Ice Freeboard Retrieval from Envisat Altimetry Data. *Remote Sens.* **2021**, *13*, 1414. [[CrossRef](#)]
42. Mallett, R.D.C.; Lawrence, I.R.; Stroeve, J.C.; Landy, J.C.; Tsamados, M. Brief communication: Conventional assumptions involving the speed of radar waves in snow introduce systematic underestimates to sea ice thickness and seasonal growth rate estimates. *Cryosphere* **2020**, *14*, 251–260. [[CrossRef](#)]

**Disclaimer/Publisher’s Note:** The statements, opinions and data contained in all publications are solely those of the individual author(s) and contributor(s) and not of MDPI and/or the editor(s). MDPI and/or the editor(s) disclaim responsibility for any injury to people or property resulting from any ideas, methods, instructions or products referred to in the content.